Department of Energy Tehnology
Aalborg University, Denmark

Control of a saturated Permanent Magnet Synchronus Motor

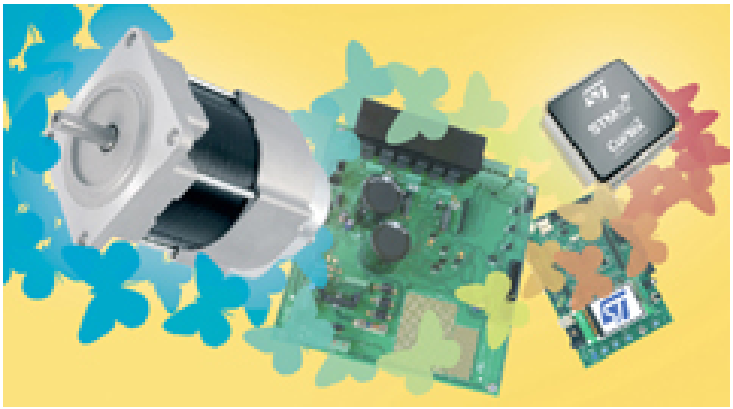

Conducted by PED 1034

Spring Semester, 2010

AALBORG UNIVERSITET

Institute of Energy Technology
Pontoppidanstræde 101
Phone number 99 40 92 47
Fax 98 15 14 11
http://www.iet.aau.dk/

Title: Control of a saturated Permanent Magnet Synchronus Motor
Semester: 4rd semester
Semester Theme: Master Thesis
Project period: 01.02.2010 to 05.06.2010
ECTS: 30
Project group: PED 1034
Members:

Adrian Opritescu

Supervisor: Kaiyuan Lu

Number of prints: 3
Number of pages: 68
Finished: 02.06.2010

Abstract:

The interest in electrical machines is spread in a large area of applications.
For this reason the purpose of this project is to investigate the nonlinear phenomenon in buried permanent magnet synchronous machine.
There is a difference in the direct and quadrature inductance of the machines. The inductance variation is investigated to observe the saliency which is based on the inductance in the d and q axis of machine. The d-axis inductance and q-axis inductance and torque are determined from a static test.
A model of the IPMSM whitch include saturation is done. The model is based on laboratory data. Field Oriented Control was implemented and tested on the IPMSM.
For validating the control, the laboratory and simulations results are compared.

By signing this document, each member of the group confirms that all participated in the project work and thereby all members are collectively liable for the content of the report.

Preface

This 4th semester report was conducted at the Institute of Energy Technology. It was written by group PED 1034 during the period from 1st of February to 02nd of June 2010.

The project theme with title *Control of a saturated Permanent Magnet Synchronus Motor* was chosen from the proposals intended for students in the 4th semester.

Reading Instructions

- The main report can be read as a self-contained work, while the appendixes contains details about M-files, and simulation
- In this project the chapters are consecutive numbered.
- Figures, equations and tables are numbered in succession within the chapters.
- Matlab and Simulink are used for all the simulations.
- Literature references are mentioned in square brackets by numbers.
- Detailed information about literature is presented in the bibliography.
- Appendixes are assigned with letters.
- A CD-ROM containing the main report and appendixes is attached to the project.

Acknowledgments:

I would like to express my gratitude to Kaiyuan Lu for his patience and his advices who many time allowed the work to be proceeded. Also I would like to thank to Octavian Oprea for his support and guidance during project work.

Summary

This project studies the control of a saturated permanent magnet synchronous machine and the present report is structured in five chapters.

Introductory chapter include information about the motor and the working principle. The main objectives and limitations are also presented.

In order to obtain the desired control, it is necessary to know the mathematically system which can be implemented. Therefore, the second chapter includes the equations and the reference frame transformation, implemented in simulations. In the last part of the chapter tests at different condition are made.

In the third chapter different control strategies and control properties are described. Maximum Torque Per Ampere and Field Oriented Control were chosen to be used in simulation. Here the controllers design and the control performances are shown.

In chapter four the laboratory work is presented. It starts with the description of the test and the setup used and further on the results obtained are shown and commented in comparison with the ones obtained from simulation. In the last chapter the conclusions are presented and also ideas for future work are shown.

All the abbreviations used in the report are included in the Nomenclature and Acronyms. The report ends with the bibliography and the M-files used for the results obtained.

Contents

List of Figures

Chapter 1

Introduction

Nowadays, two of the main research objectives are regarding the energy savings and proper management of the energy resources.

In energy savings, the apparatus are designed and manufactured in order to reduce the energy consumption. For this purpose the efficiency was increased, i.e. the equipment that provides maximum performance while using minimum energy.

In electrical machine the efficiency has been improved also, by changing the machine type, structure or improving the control of the machine. Electrical machines started to become simpler, reliable and less expensive in order to improve the selling capability. Variable speed drives has increased, being used in application like: robotics, electric cars and air conditioning.

Synchronous machines are used now for application ranging from high power to low power. From this class of machines Permanent Magnet Synchronous Machines (PMSM) are very advantageous and challenging.

The advantage consists due to the reluctance torque and to several features like high efficiency, high power factor, and high controllability on an extended speed range. Also since the rare earth PM material and technology has reduced the price of the magnets, PMSM are available on the market at low cost[1].
Weight and seize have been reduced, keeping the same output power. Lower the mass the rotor inertia will decrease resulting in better dynamic response.

In permanent magnet machines if the magnets are placed in the interior of the rotor the motor is called Interior Permanent Magnet Synchronous Motor (IPMSM).
An important disadvantage of the IPMSM is represented by the effect of magnetic saturation. Magnetic saturation affects the motor performance and also its control within the drive system. The effect of magnetic saturation has been investigated by many researchers, but assumptions were done in all the cases.
For example in some models the cross saturation phenomenon is not included or L_d and L_q inductance are considered equal. There are also models where only a single saturation factor approach is included or models used to estimate the q axis inductance while d axis inductance was constant. More information about this work can be found in [4],[5],[6].

In this project an investigation for the effect of magnetic saturation for an IPMSM is done in order to represent the saturation effects on L_d, L_q who are functions of saturation level. Because of the magnetic saturation, the flux cannot be expressed as functions of inductances. Each flux is a nonlinear function of the currents.

In the next section additional information and classification about the PMSM is given.

1.1 Permanent Magnet Motors

Permanent Magnet Synchronus Motors (PMSM) are attractive growing for a wide range of industrial drives and servo applications.

A permanent magnet synchronous electrical machine (PMSM) is a rotating electric machine used to convert electrical energy into mechanical energy. First, the electrical energy is converted in magnetic energy and finally the magnetic energy is converted into mechanical energy.

The most common materials used to manufacture the rotor are the ferrite and rare earth magnets. The ferrite is cheap and generates a weak magnetic flux while the rare earth magnets are expensive and generate a strong magnetic flux [7].

Using rare magnets a high torque to weight ratio and high efficiency can be achieved. The power of the PMSM is defined as:

$$P_m = \omega_m \cdot T_e \tag{1.1}$$

where P_m is the mechanical power generated by the motor, ω_m is the mechanical speed of the shaft (rotor) [rad/s], T_e is the generated torque [Nm]. The mechanical power will always be smaller than the electrical power used by the motor.

1.1.1 Classification of PM Motors

A simple classification can be seen in Fig 1.1. PM motors can be divided in two groups: AC and DC machines. The only difference between PMDC and conventional DC machines is the use of permanent magnets in the place of field windings.

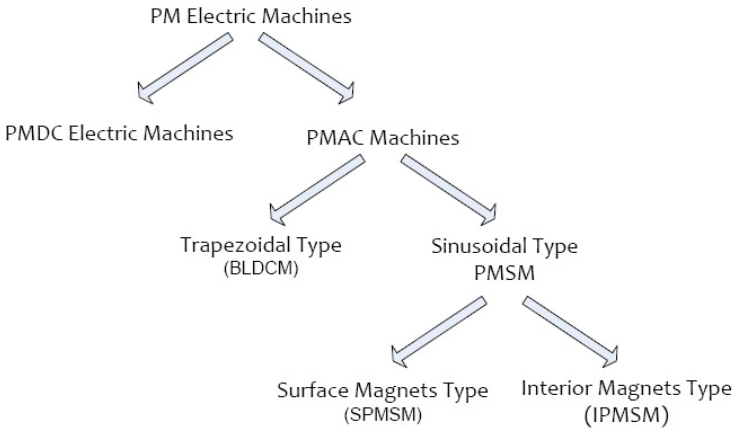

Figure 1.1: *Classification of PM electric machines [1]*

The PMAC are very simple since the comutator and brushes don't exist. The field is generated by the magnets placed in the rotor. The PMAC machines are grouped in trapezoidal and sinusoidal type. They are called like this in function of the back-EMF voltage waveform induced in each stator phase [1].

The sinusoidal PMAC machines started to be more used due to the superior power density, high torque to inertia ratio, efficiency, and availability of high density permanent magnet material at relatively low cost [1].

The distribution of air gap flux density in permanent magnet synchronous machine, with load, has a distorted waveform caused by the saturation effect on the rotor. The extent of saturation along d and q axes also varies according to the type of rotor configuration [3].

In function on how are the magnets placed in the rotor, two main types can be distinguish in Fig 1.2: a) surface magnet type b)interior magnet type.

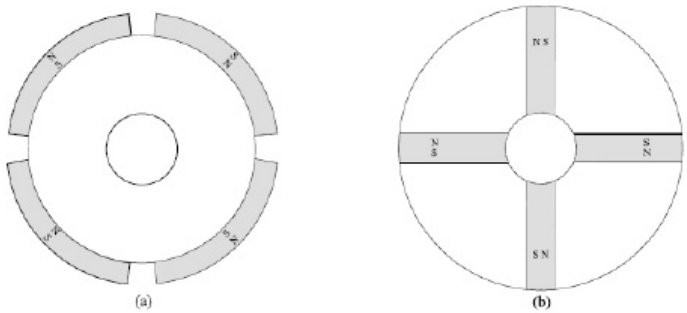

Figure 1.2: *PMSM rotor types [7]*

The surface mounted permanent magnet is a non salient machine since the permeability of the magnet material is similar with air permeability.
This configuration presents a high reluctance path to magnetizing flux that does not vary much with position around the rotor causing the d and q axes inductance difference to be insignificant [3].

The IPMSM are more robust and can operate at higher speed. When the magnets are buried inside the rotor, saliency effect appears where saliency can be defined as the nonuniformity of the air gap between rotor and stator. Because of the rotor magnets and saliency, cogging torque also arise in IPMSM, where cogging torque represents the parasitic tendency of the rotor to align in connections with action of the magnet at discrete positions [2].

For this machine, direct axis reactance is bigger than quadrature axis reactance $X_q \prec X_d$. The reason for this is that in the magnetic circuit of the quadrature axis is only iron but a part of the magnetic circuit in the direct axis of the rotor consists of the magnet whose permeability is almost equal to air permeability [2]. Thus the d axis reluctance is increased and its reactance is decreased.

1.1.2 Working principle

The PMSM stator is similar to an induction machine or switched reluctance machine stator, with the main difference the rotor. The induction machine has wound or squirrel cage rotor, the switched reluctance machine has an iron core rotor and the PMSM rotor is mainly made of permanent magnets and ion laminations.

The three stator windings are placed 120°apart with respect to each other. In the figure below the placement of the stator winding for a three phase machine with two poles per phase can be seen.

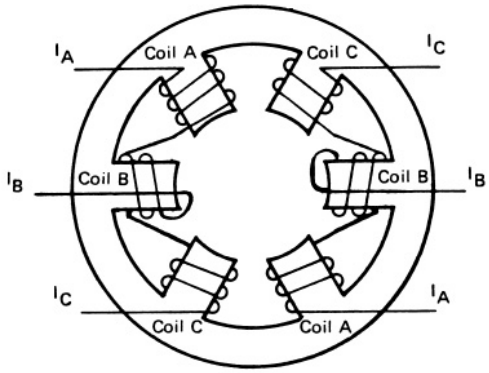

Figure 1.3: *PMSM with 2 poles [8]*

In Fig 1.4 can be seen how the magnetic field generated by electromagnets interacts with the magnetic field generated by the permanent magnet, resulting in rotational movement of the magnet. Two magnetic poles of the same sign will always push against each other while two magnetic poles of different sign will always attract each other.

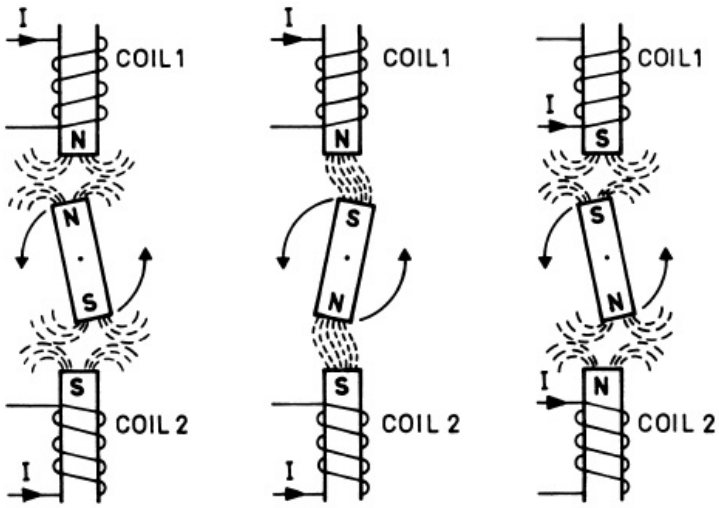

Figure 1.4: *Working principle [8]*

The principle behind the operation of the PMSM is the interaction between the rotating magnetic field generated by the stator and the magnetic field generated by the rotor.

An advantage of the PMSM is the generation of the rotor flux by the permanent magnets without needing the use of electrical energy.

By supplying the stator windings with voltage the resultant magnetic field generated by the stator will rotate. The rotating speed of the resultant magnetic field is proportional to the frequency of the supply voltages and is called the synchronous speed [8].

The synchronous speed is calculated using the following formula:

$$n_s = \frac{120 \cdot f}{n} \tag{1.2}$$

where n_s is the synchronous speed [rad/s], f is the frequency of the supply voltage [Hz], n is the number of poles per phase.

From the above equation it can be seen that synchronous speed is dependent on the frequency and the number of poles per phase. The synchronous speed will decrease if the number of poles increase. The rotor of a PMSM is rotating with synchronous speed. For this reason the PMSM is used where precise control of the speed is necessary.

The mechanical speed depends on the number of pole pairs per phase and synchronous speed. The formula used to calculate the mechanical speed is the following:

$$\omega_e = \omega_m \cdot n_{pp} \tag{1.3}$$

where ω_e is the electrical speed of the rotor [rad/s], ω_m is the mechanical speed of the rotor [rad/s], n_{pp} is the number of pole pairs per phase.

1.2 Project Objectives

The main goal of this project is to determine and test an IPMSM considering the saturation effect.

The main requirements of the project are:

- Analysis and determination of IPMSM parameters.
- Investigation on saturation effects.
- Test results on a lab setup with verification of analysis and design work.
- Choosing the matematichal model for IPMSM.
- Control of IPMSM in order to determine the corectness of the model.

1.3 Project Limitations

During project development, several limitations had to be imposed. This project will be focus on laboratory measurements and modeling of the saturated IPMSM. The dynamic control of the motor using D-space platform will not be implemented.

The main limitations of the project are:

- Only the IPMSM model will be consider.
- Measurements are done only under static tests.
- Real system dynamic control will not be implemented

Chapter 2

Mathematical model

In this chapter the equations of the motor are presented in order to understand the physics and to have the necessary knowledge to design the control of the electrical machine. The mathematical model will be further tested using these equations.

2.1 Voltage equations in the stationary a,b,c reference frame

The stator voltage equations of the PMSM in natural a,b,c reference frame can be expressed in matrix form as below [1]:

$$v_{abcs} = r_s i_{abcs} + i_{abcs} + \frac{d}{dt}\lambda_{abcs} \tag{2.1}$$

where, r_s is the the stator winding resistance per phase, i_{abcs} is the stator phase current matrix, v_{abcs} is the stator phase voltage matrix and λ_{abcs} is the stator flux linkage matrix. All the matrix the can be seen in 2.2.

$$v_{abcs} = \begin{bmatrix} v_{as} \\ v_{bs} \\ v_{cs} \end{bmatrix}; i_{abcs} = \begin{bmatrix} i_{as} \\ i_{bs} \\ {}_{cs} \end{bmatrix}; \lambda_{abcs} = \begin{bmatrix} \lambda_{as} \\ \lambda_{bs} \\ \lambda_{cs} \end{bmatrix} \tag{2.2}$$

The flux linkage matrix λ_{abcs} include the stator currents and rotor permanent magnet flux in below matrix.

$$\lambda_{abcs} = \lambda_{abcs(s)} + \lambda_{abcs(r)} \tag{2.3}$$

where $\lambda_{abcs(s)}$ and $\lambda_{abcs(r)}$ are defined as:

$$\lambda_{abcs(s)} = \begin{bmatrix} L_{aas} & L_{abs} & L_{acs} \\ L_{bas} & L_{bbs} & L_{bcs} \\ L_{cas} & L_{cbs} & L_{ccs} \end{bmatrix} i_{abcs} \quad ; \quad \lambda_{abcs(r)} = \lambda_m \begin{bmatrix} sin(\theta_r) \\ sin(\theta_r - \frac{2\pi}{3}) \\ sin(\theta_r + \frac{2\pi}{3}) \end{bmatrix} \tag{2.4}$$

In equation 2.4, θ_r is the rotor position angle, L_{aas}, L_{bbs}, L_{ccs} are the self inductance of phase a, b, c, λ_m represent the amplitude of the flux linkage and L_{abs}, L_{acs} are the mutual inductances between two phases. Because of the rotor saliency in IPMSM the air gap is not uniform and therefore the self and mutual inductances of stator windings are a function of the rotor position [1].

The self and mutual inductances can be seen in equations below .

$$L_{aas} = L_{ls} + L_A - L_B cos2\theta_r \tag{2.5}$$

$$L_{bbs} = L_{ls} + L_A - L_B cos(2\theta_r + \frac{2\pi}{3}) \tag{2.6}$$

$$L_{ccs} = L_{ls} + L_A - L_B cos(2\theta_r - \frac{2\pi}{3}) \tag{2.7}$$

$$L_{abs} = L_{bas} = -\frac{1}{2}L_A - L_B cos(2\theta_r - \frac{2\pi}{3}) \tag{2.8}$$

$$L_{acs} = L_{cas} = -\frac{1}{2}L_A - L_B cos(2\theta_r + \frac{2\pi}{3}) \tag{2.9}$$

$$L_{bcs} = L_{cbs} = -\frac{1}{2}L_A - L_B cos2\theta_r \tag{2.10}$$

Finally the flux linkage matrix λ_{abcs} can be expressed as in equation 2.11

$$\begin{bmatrix} \lambda_{as} \\ \lambda_{bs} \\ \lambda_{cs} \end{bmatrix} = L \begin{bmatrix} i_{as} \\ i_{bs} \\ i_{cs} \end{bmatrix} + \begin{bmatrix} sin(\theta_r) \\ sin(\theta_r - \frac{2\pi}{3}) \\ sin(\theta_r + \frac{2\pi}{3}) \end{bmatrix} \lambda_m \tag{2.11}$$

2.2 Voltage equations in rotor d,q reference frame

The voltage equations expressed in a,b,c reference frame can be written in a compact form by using the space vectors. The space vector approach is still not a simple model but mathematical simplification can be made if the space vector model referred to a rotating reference frame. All the reference frame transformation are described in Section 2.5.

Finally the rotor reference frame voltage vector is given as in equation 2.12, where superscript r is used for quantities of rotor reference frame [1]. The rotor position dependent terms are eliminated by transforming the flux linkage vector to the rotor dq reference frame. This is the main advantage for equations in rotor reference frame.

$$\underline{v}^r_{sqd} = r_s \underline{i}^r_{sqd} + \frac{d}{dt}\underline{\lambda}^r_{sqd} + j\omega_e \underline{\lambda}^r_{sqd} \tag{2.12}$$

The flux linkage vector in rotor reference frame is obtained from equation 2.13.

$$\underline{\lambda}^r_{sqd} = \underline{\lambda}_{sqd} e^{-j\theta_r} \tag{2.13}$$

In equation 2.14 the flux linkage vector is written using the magnetizing inductances L_{md} and L_{mq} [1].

$$\underline{\lambda}^r_{sqd} = (L_{ls} + \frac{L_{md} + L_{mq}}{2})\underline{i}^r_{sqd} - \frac{L_{md} + L_{mq}}{2}\underline{i}^r_{sqd} * + \lambda_m e^{-j\frac{\pi}{2}} \tag{2.14}$$

The expresions for magnetizing inductances are defined in equation 2.15.

$$L_{md} = \frac{3}{2}(L_A + L_B); L_{mq} = \frac{3}{2}(L_A - L_B) \tag{2.15}$$

$$L_A = \frac{L_{md} + L_{mq}}{3}; L_B = \frac{L_{md} - L_{mq}}{3} \tag{2.16}$$

$$\underline{v}^r_{sqd} = v^r_{sq} - jv^r_{sd}; \quad \underline{i}^r_{sqd} = i^r_{sq} - ji^r_{sd}; \quad \underline{\lambda}^r_{sqd} = \lambda^r_{sq} - j\lambda^r_{sd} \tag{2.17}$$

Substituting the expressions from 2.17 to 2.12 and 2.14 and equating the real and imaginary parts in both sides of the equations the scalar form of the machine equations is obtained as in 2.18 and 2.19.

$$v^r_{sq} = r_s i^r_{sq} + \frac{d}{dt}\lambda^r_{sq} + \omega_e \lambda^r_{sd} \tag{2.18}$$

$$v_{sd}^r = r_s i_{sd}^r + \frac{d}{dt}\lambda_{sd}^r - \omega_e \lambda_{sq}^r \tag{2.19}$$

The flux linkage used in the above equations are defined as in 2.20.

$$\lambda_{sq}^r = L_q i_{sq}^r; \qquad \lambda_{sd}^r = L_d i_{sd}^r + \lambda_m \tag{2.20}$$

2.3 The electromagnetic torque

The electromagnetic torque can be obtained from the power balace equation of the machine. The instantaneous power p_e flowing into the machine can be written from rotor dq frame variables as in 2.21[1]:

$$p_e = \frac{3}{2}(v_{sd}^r i_{sd}^r + v_{sq}^r i_{sq}^r) \tag{2.21}$$

Substituting the equations 2.19 and 2.18 into 2.21 the new expression for the instantaneous power p_e is obtained. The first term from 2.22 represent the power loss in the conductors, the second term is the time rate of change of stored energy in the magnetic field and the last term represent the energy conversion. [1]

$$p_e = \frac{3}{2}[r_s {i_{sd}^r}^2 + r_s {i_{sq}^r}^2] + \frac{3}{2}[\frac{d}{dt}L_d \frac{{i_{sd}^r}^2}{2} + \frac{d}{dt}L_d \frac{{i_{sd}^r}^2}{2}] + \frac{3}{2}[\omega_e \lambda_{sd}^r i_{sq}^r - \omega_e \lambda_{sq}^r i_{sd}^r] \tag{2.22}$$

The last term is the p_{em} and represent the electromechanical power.

$$p_{em} = \frac{3}{2}[\omega_e \lambda_{sd}^r i_{sq}^r - \omega_e \lambda_{sq}^r i_{sd}^r] \tag{2.23}$$

Multiplying the mechanical speed ω_m and the torque T_e produced from the machine, the electromechanical power can be written like in 2.24. The relationsheep between mechanical and electrical speed is also given in equation 2.24.

$$\omega_m T_e = \frac{3}{2}[\omega_e \lambda_{sd}^r i_{sq}^r - \omega_e \lambda_{sq}^r i_{sd}^r]; \qquad \omega_e = \frac{n}{2}\omega_m \tag{2.24}$$

Finally substituting the flux linkage from 2.20 the torque expression is obtained as below.

$$T_e = \frac{3}{2}\frac{n}{2}[\lambda_{sd}^r i_{sq}^r - \lambda_{sq}^r i_{sd}^r] \tag{2.25}$$

2.4 Mechanical equation of the machine

The mechanical equation express the relationship between the electromagnetic torque T_e, load torque T_l and electrical speed ω_e, where J is the rotor inertia and B_m is the viscous friction coefficient.

$$T_e = J\frac{2}{n}\frac{d}{dt}\omega e + B_m \frac{2}{n}\omega_e + T_l \tag{2.26}$$

The equations presented in this section are used in the simulation part in order to see the behavior of the machine under different condition.

2.5 Reference frame transformation

The dq transformation is done from the three phase stationary coordinate system to rotating dq coordinate system. In order to make the transformation in a easier manner it is necessary to work in two steps:

- The three phase stationary abc system is transformed in two phase stationary system $\alpha\beta$ also known as Clarke Transformation.
- The two phase stationary coordinate system is transformed in dq rotating system also known as Park Transformation.

2.5.1 Clarke Transformation, from abc to $\alpha\beta$

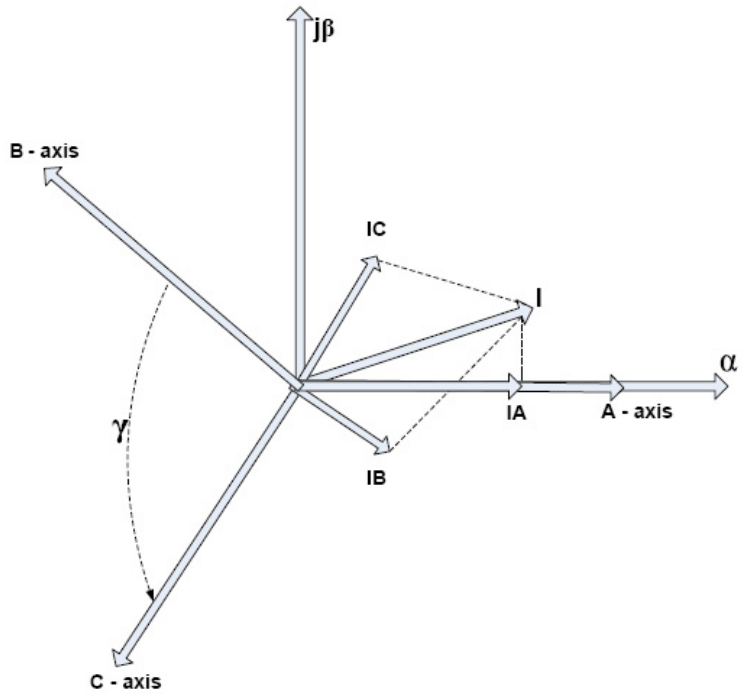

Figure 2.1: *The current space vector in α β*

In Fig 2.1 can be observed how the magnetic axes of the three phase machine are separated by angle γ=$\frac{2}{3}$. Phase A is arbitrary chosen to coincide with α from the new coordinate system and β leads α with 90°. In order to obtain the phase currents is necessary to project the current space vector on the phase axis. The transformation is given in the following matrix:

$$\frac{2}{3} \cdot \begin{bmatrix} 1 & cos(\gamma) & cos(2\gamma) \\ 0 & sin(\gamma) & sin(2\gamma) \end{bmatrix} \cdot \begin{bmatrix} i_{A(t)} \\ i_{B(t)} \\ i_{C(t)} \end{bmatrix} = \begin{bmatrix} i_{\alpha(t)} \\ i_{\beta(t)} \end{bmatrix} \tag{2.27}$$

For voltage and flux linkage the transformations are the same. The equation 2.27 can be written in compact way as below:

$$i_{\alpha\beta(t)} = \frac{2}{3}[i_{A(t)} + i_{B(t)} \cdot a + i_{C(t)} \cdot a^2] \tag{2.28}$$

where a= cos(γ)+jsin(γ) is a vector operator that make the vector rotation [1].

In 2.29 the current space vector is defined in complex coordinates:

$$i_{\alpha\beta(t)} = i_{\alpha(t)} + ji_{\beta(t)} \tag{2.29}$$

2.5.2 Park Transformation(from $\alpha\beta$ to dq)

For electric machines it is necessary to adopt a common reference frame for both rotor and stator. Thus it is necessary to define the vector rotation where the space vectors are rotated through a known angle [11].

In Fig 2.2 the current is drawn in stationary coordinates. If the current is rotating in anti clockwise direction , then the dq reference frame will rotate in the same direction with the current space vector and with the same speed. The current space vector in rotating reference frame is shown below:

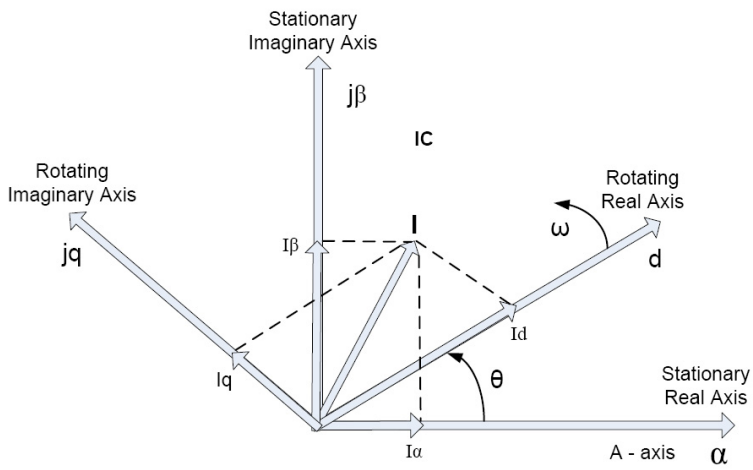

Figure 2.2: *The current space vector in rotating reference frame*

The quadrature axes and the current space vector are rotating at a speed ω, but from rotating point of view the current space vector is stationary. The current space vector in rotating reference frame is given in 2.30.

$$\begin{bmatrix} cos(\theta) & sin(\theta) \\ -sin(\theta) & cos(\theta) \end{bmatrix} \cdot \begin{bmatrix} i_\alpha \\ i_\beta \end{bmatrix} = \begin{bmatrix} i_d \\ i_q \end{bmatrix} \tag{2.30}$$

and can also be writen like as:

$$i_{dq} = i_d + ji_q = ie^{-j\theta} \tag{2.31}$$

Wwhere θ is the angle between the real axis of the rotating reference frame and the real axis of the stationary reference frame.

2.6 Simulation of the IPMSM

The IPMSM mathematical model is implemented in Simulink to validate the machine model at different torque levels. The structure model can be seen in Fig 2.3 and the Simulink model is included in Appendix A.

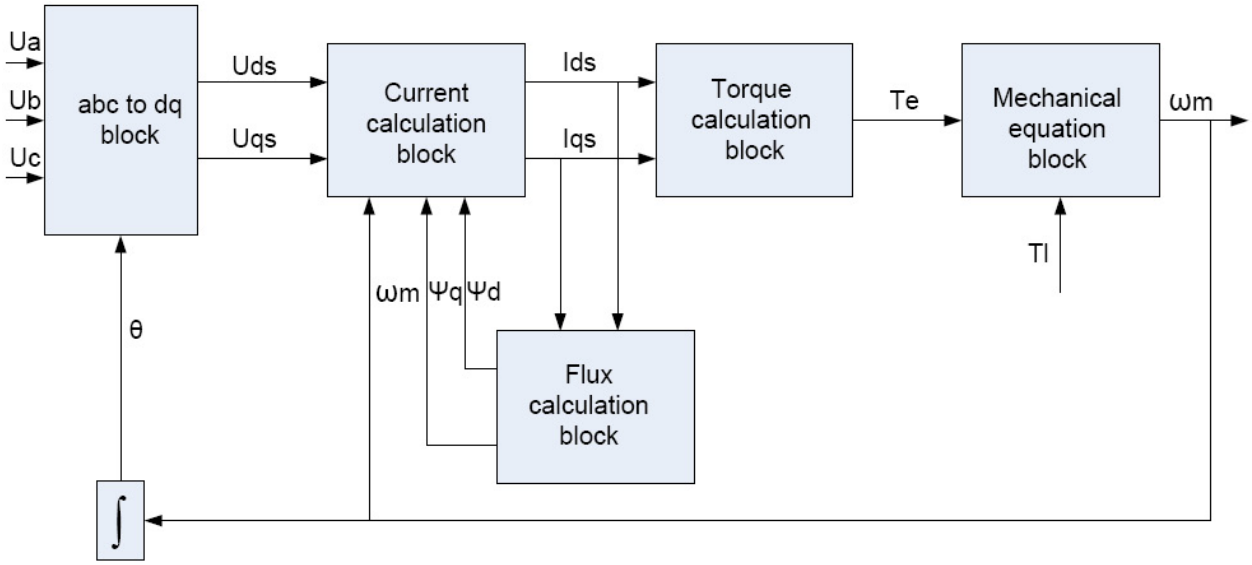

Figure 2.3: *Scheme of IPMSM simulated model*

The inputs of the first block from Fig 2.3 are the phase voltages. Using the transformation presented in Section 2.5 the dq voltages are obtained. The stator current in reference frame coordinates are derived from the measured stator voltage and from the dq fluxes. The electrical speed used in the calculation of the currents is taken from the output of the mechanical equation block.

Next the d and q currents are used as inputs for the electromagnetic torque calculation block, based on the equation 2.25. Finally the mechanical speed is obtained as output of the machine model by using the electromagnetic torque and load torque as inputs in equation 2.26.

Integrating the mechanical speed , the rotor position is found necessary in the voltage transformation block. Next the blocks used in simulation are presented. In Fig 2.4 the current calculation block is presented.

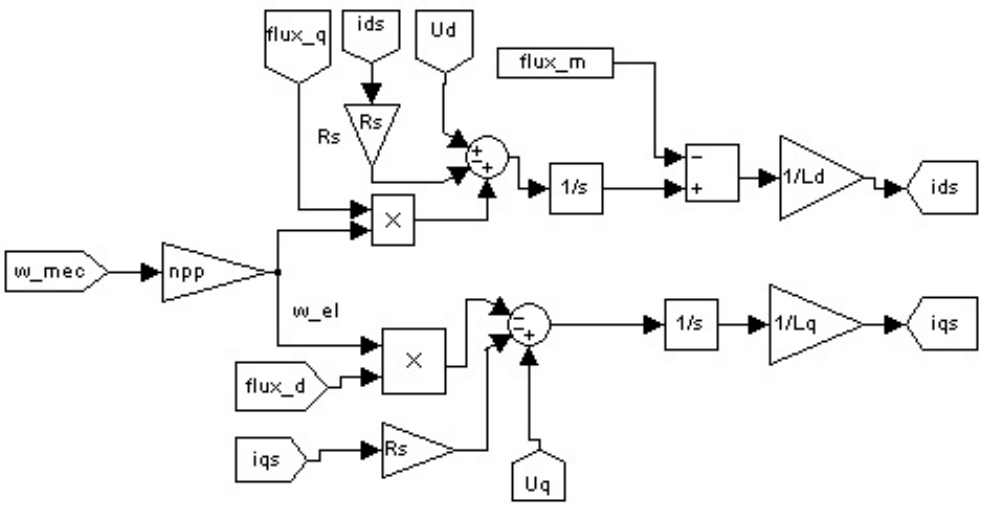

Figure 2.4: *Model of the currents calculation blocks implemented in Simulink*

In Fig 2.5 the flux linkage calculation block can be seen.

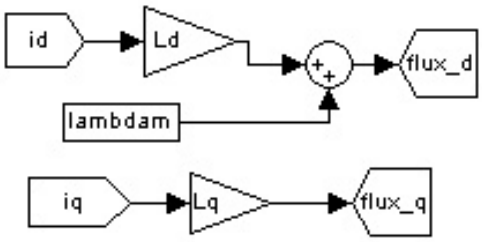

Figure 2.5: *Model of the flux linkage calculation block implemented in Simulink*

In Fig 2.6 the electromagnetic torque calculation block is presented.

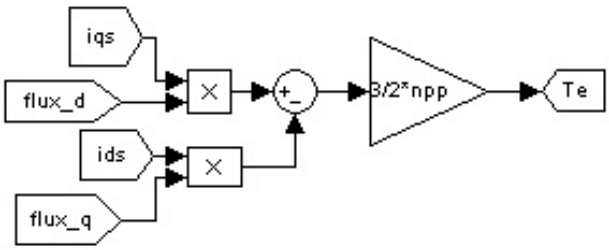

Figure 2.6: *Model of the electromagnetic torque calculation block implemented in Simulink*

Finally in Fig 2.7 the mechanical equation block is shown.

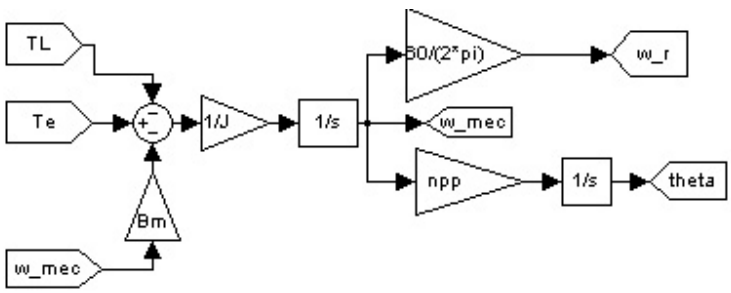

Figure 2.7: *Model of the mechanical equation calculation block implemented in Simulink*

The motor tested in the laboratory is a IPMSM. All the motor parameters used for the simulation are included in Table 2.1.

Table 2.1: *IPMSM electric parameters*

Parameter	Simbol	Value	Unit
Stator resistance	R_s	0.11	[ohm]
D-axis inductance	L_d	3.2	[mH]
Q-axis inductance	L_q	4.1	[mH]
Number of pole pairs	npp	3	-
PM flux linkage	ψ_m	0.08	[Wb]
Nominal speed	ω_m	4200	[rpm]
Line to line voltage	V	193.5	[V]
Line to line peak voltage	V	41	[V]
Nominal torque	T	15	[Nm]
Nominal power	P	6597	[W]
Moment of inertia	J	0,00032	[kgm^2]

2.6.1 Simulation results

The IPMSM was tested for a reference speed of 4200[rpm] with a load torque equal with zero. At 0.4 seconds a step to rated load torque(Tl=15Nm) is applied to the machine. In Fig 2.8 at nominal speed can be observed how the measured speed is following the reference speed. When the load torque is applied a small perturbation of the speed can be observed.

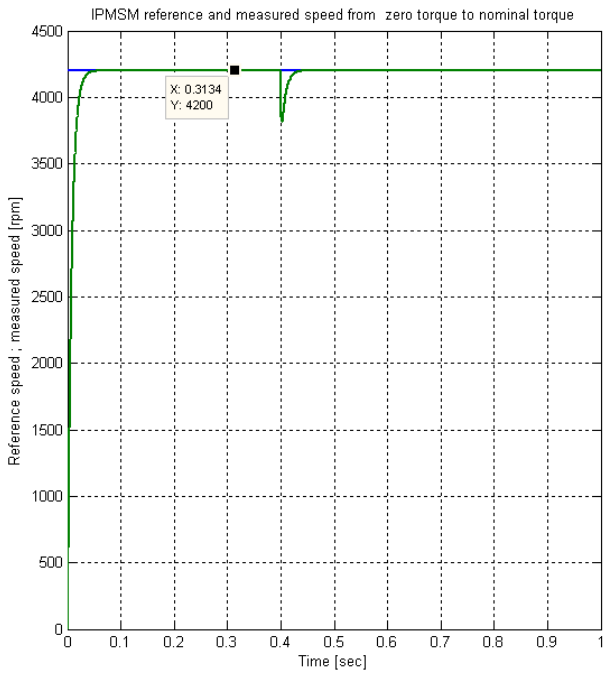

Figure 2.8: *Measured and reference speed response at full load*

In Fig 2.9 can be seen that I_d and I_q currents are zero when the load torque is zero. After 0.4 sec,when the machine is driven at rated speed, rated load torque, the value of I_q current is equal with 41.66[A].

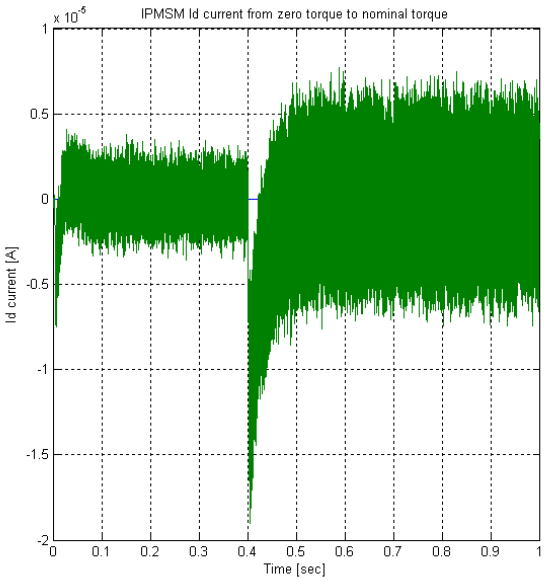

(a) Id current response

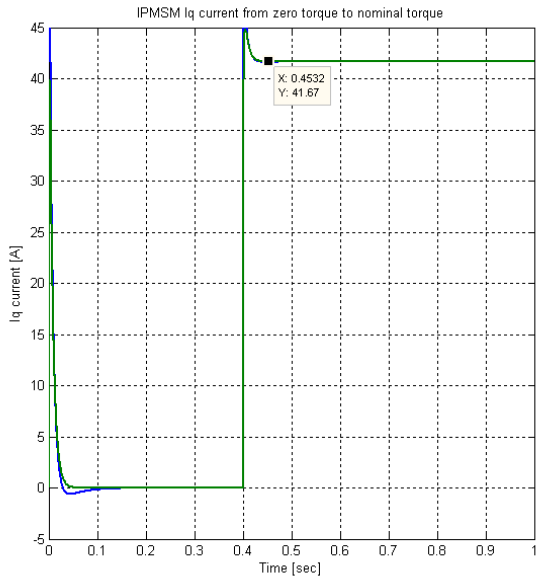

(b) Iq current response

Figure 2.9: *I_d and I_q currents response at rated speed, rated load torgue*

In Fig 2.10 the stator current and voltages are shown. When machine is running at rated speed and zero load torque, the current is zero as expected. When the machine is working at rated load torque the amplitude of the current has the value 41.6[A]. The stator voltage at rated speed and zero load torque has the value 100[V] and at rated speed, rated torque it has the value 246[V], as shown also in the datasheet. Using the rated current the torque can be calculated as in equation 2.25. Calculating the torque which is equal with $T = 3/2 \cdot 3 \cdot 0.08 \cdot 41.6 \cong 15[Nm]$, shows the corectness of the simulation.

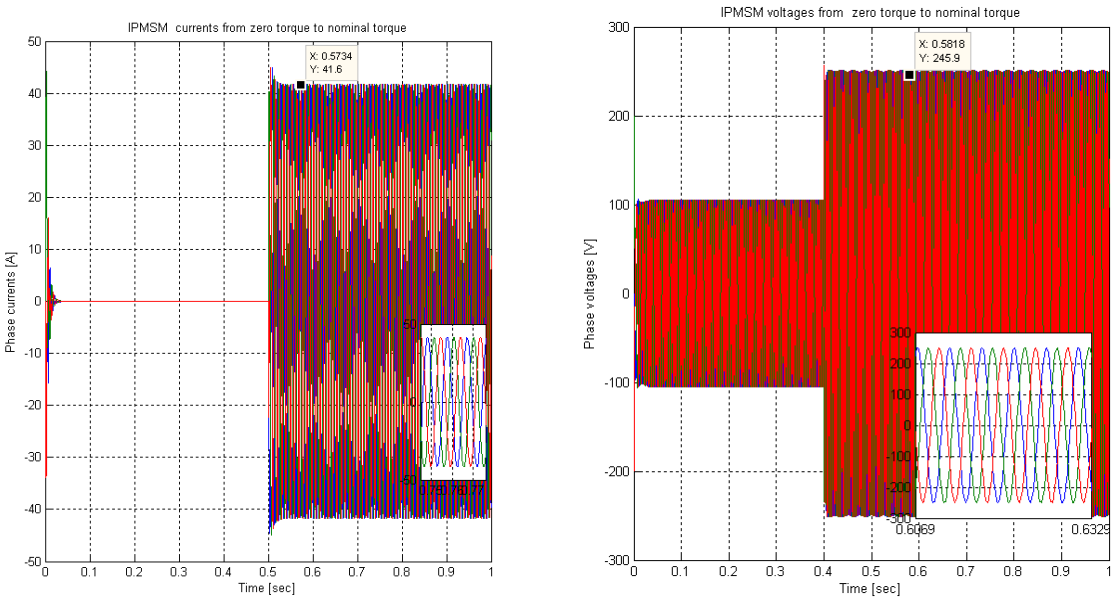

(a) Current response

(b) Voltage response

Figure 2.10: *Currents, voltages response from zero to nominal load torque*

In this chapter the mathematical model of IPMSM and reference frame transformation were presented. To test the performances of the machine the model was implemented in Matlab/Simulink software. Using this simulation, the machine was validated at rated speed, rated load torque, and the results are showing the validation of the model.

Next chapter will describe and implement the control of the machine in simulation.

Chapter 3

Motor Control

Control techniques for permanent magnet motor are presented in this chapter. These techniques are grouped in two sections: scalar and vector control. In the scalar control amplitude and frequency are controlled. In vector control position of space vector and amplitude are considered.

There are two commonly used control methods for PMSM: Direct Torque Control(DTC) and Field Oriented Control(FOC). The two control strategies works based on different principles but with the same purpose: the control of the torque and flux in order to have the motor fallowing the command trajectory. The control should be robust for different disturbances or load parameters changes.

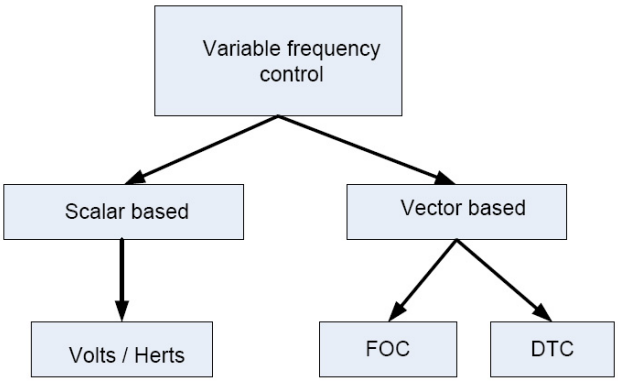

Figure 3.1: *Control method used for PMSM*

3.1 Volt/frequency control

Volt/frequency control, known as scalar control is one of the most simples methods used to control the motors. The simplicity is coming from the fact that the control is made in open loop scheme and is not using any feedback loop. The open loop is used in order to avoid changes in speed command and in case if load is being changed losses of synchronization can appear in PMSM.

Current and torque are not controlled, instead voltage and frequency are becoming the controlled variables. The principle is based on keeping the stator flux constant at rated value for the motor to develop rated torque/ampere ratio over entire speed range. A sinusoidal voltage PWM algorithm is implemented to increase the amplitude of fundamental voltage [1].

Therefore the dynamic performance is poor, with high overshoot. The signal used in feedback loop is the rotor position needed to control the synchronization between the rotor and the field. The block diagram of V/f control can be seen in Fig 3.2.

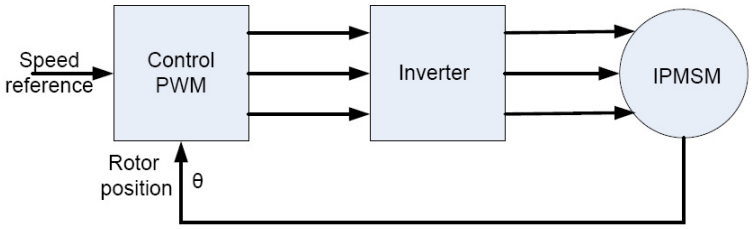

Figure 3.2: *Block diagram of V/f control*

The back EMF voltage is increased and the resistive drop can be ignored at high speed. At lower speeds to compensate the resistive drops the voltage is increased. If flux is constant the voltage becomes proportional with rotor angular frequency [1].

The advantages of using this method are: low cost, simple control, only feedback for position. There are disadvantages like: torque is not controlled directly, unsatisfactory dynamics. This strategy is not stable because does not guarantee the synchronization of the rotor with the excitation frequency [1].

3.2 Field oriented control

This strategy is implemented in synchronous machine in order to have an easier control. The algorithm is done in the rotating dq rotor reference frame, in which the currents and voltages are considered as constant values. There are 2 control loops:

- Speed loop, that controls the speed of the motor.
- Current loop for i_{sd} and i_{sq} currents who controls the torque of the motor.

Proportional integrators (PI controllers) are used because the steady state error becomes zero due to integrator term. The overall control structure is presented in Fig 3.3.

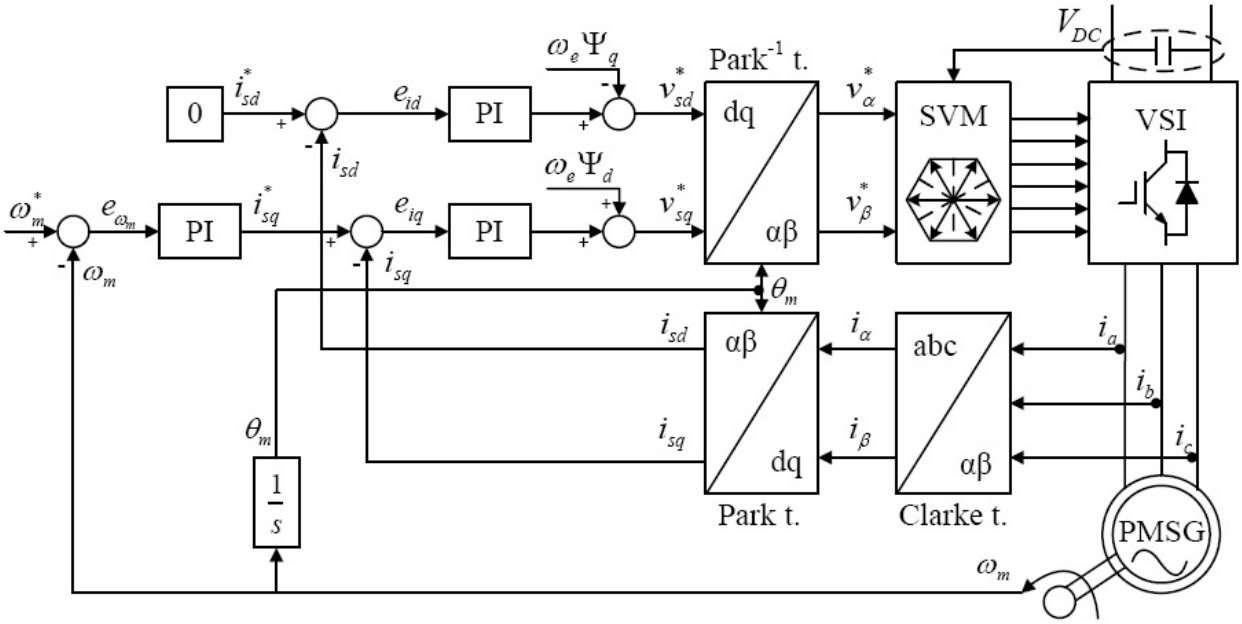

Figure 3.3: *Field Oriented Control structure block [1]*

The acquisition of the three phase stator currents, the DC link voltage and the rotor position are required. Only two current sensors are needed because the sum of the three phase currents is always zero. The d axis is aligned with the flux-linkage of the permanent magnet vector, therefore the position of PM flux is obtained by measuring the rotor speed. Integrating the rotor speed the rotor position can be found.

Using Clarke's transformation shown in Section 2.5 the currents from the abc reference frame are transformed into two dimensional stationary reference frame. Appling the Park transformation described in section 2.5 to the stator currents and knowing the rotor position the currents i_{sd} and i_{sq} are obtained.

The stator current i_{sd} is maintained at zero, for producing maximum torque. I_{sq} current is calculated from the reference torque obtained at the output of the speed PI controller. The outputs of the PI controllers together with the DC link voltage are the command values for PWM generation in Space Vector Modulator (SVM) block.

The advantages of FOC are: mechanical position, good torque response, accurate speed control, full torque at zero speed. The disadvantages are current feedback, many equations and transformations need to be implemented [1].

3.3 Direct Torque Control

In Direct Torque Control (DTC), the controlled variables are the flux linkage and torque. It can be implemented using hysteresis flux and torque control together with a switching tables or using space vector modulation (SVM) and PI controllers. Another method can be implemented by using a parallel cascade structure as seen in Fig 3.4.

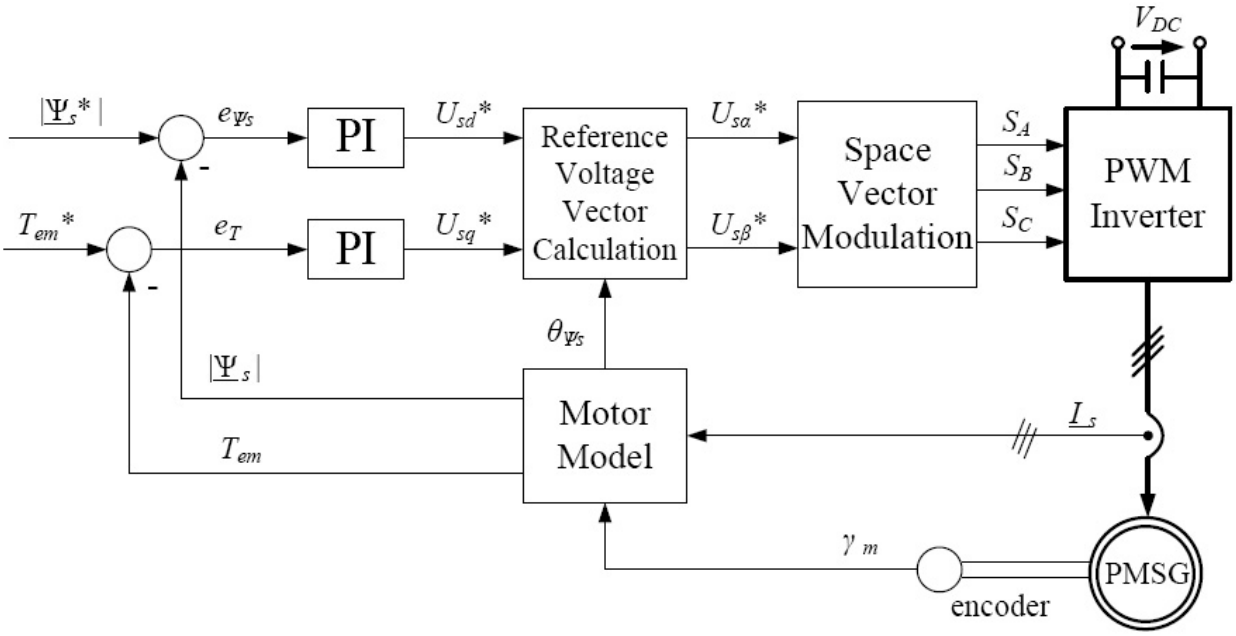

Figure 3.4: *Direct Torque Control structure block [1]*

The reference value of the stator flux Ψ_s^* is compared with the estimated value of the stator flux Ψ_s and the flux error $e_{\Psi s}$ who is the input of the flux PI controller. In the case of the torque PI controller the torque eror e_T is obtained by comparing the torque reference value T_{em}^* with the estimated value T_{em} .

From the outputs of the PI, the new voltages obtained U_{sd} and U_{sq} are delivered to the space vector modulator. Finally the signals S_a, S_b and S_c used to control the PWM converter are obtained.

DTC presents features like simple structure and a very good dynamic behavior. The main disadvantages are regarding the variable switching frequency, high torque pulsation and fast sampling time requirements.

From all the control methods presented FOC was choosen to be implemented in simulation due to the good performance obtained.

3.4 Control Property

In this section different control properties are shortly presented. These controls have different advantages and disadvantages, which result in different motor performance. The most important control properties are listed below:

- Constant torque angle
- Unity power factor
- Constant Stator Flux Control
- Maximum torque per ampere control

3.4.1 Constant torque angle

In this method the torque angle is kept constant at 90° as seen in Fig 3.5. The torque angle is defined as the angle between stator current space vector and d-axis of the rotor. Using constant torque angle strategy, the reluctance torque can not be used. This control can be achieved by controlling the d-axis current.

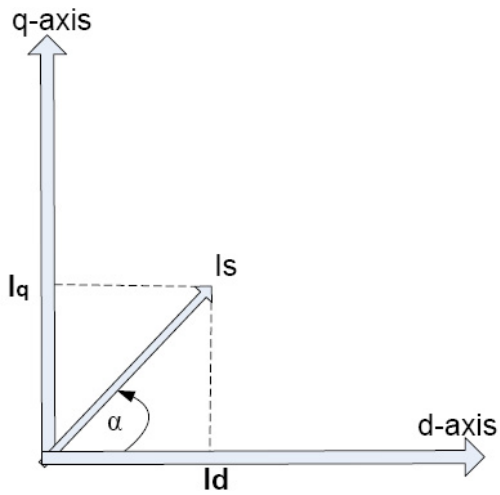

Figure 3.5: *Torque angle Alfa*

Where $i_d = |i_s|\, cos(\alpha)$ and $i_q = |i_s|\, sin(\alpha)$. Starting from torque equation presented in mathematical model chapter and including the new expression for i_d and i_q, torque equation can be obtained.

Where $i_d = 0 \Rightarrow |i_s| = i_q$.

$$T_e = \frac{3}{2}\frac{n}{2}\lambda_m i_q \tag{3.1}$$

This method is one of the easiest control strategies. The most important advantage is the direct proportionality between torque and current. A drawback of this method is reluctance torque, which is not used.

3.4.2 Unity power factor

With this method the power factor in maintained at unity, by keeping the power factor angle $\varphi = 0$. The volt-ampere rating is minimized but the maximum torque and efficiency are smaller. The power factor expression is shown below:

$$PF = cos(\phi) = cos(\angle i_s - \angle v_s) \tag{3.2}$$

where I_s is the current vector and v_s is the voltage vector.

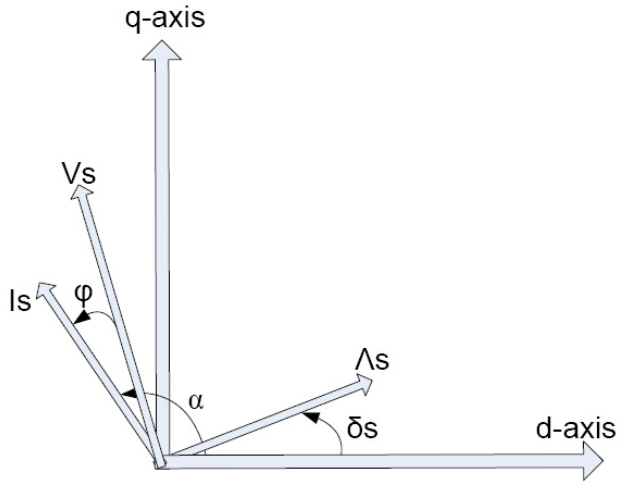

Figure 3.6: *Diagram of vectors and vectors angle*

From Fig 3.6, current vector i_s and stator flux linkage λ_s are perpendicular and the current expression can be derived.

$$i_d = -\left|i_s\right| sin(\delta_s) \tag{3.3}$$

$$i_s = \left|i_s\right| cos(\delta_s) \tag{3.4}$$

$$\Rightarrow tan(\delta_s) = \frac{sin(\delta_s)}{cos(\delta_s)} = -\frac{i_d}{i_q} \tag{3.5}$$

Where δ_s is the angle of stator flux linkage vector. Starting from the above equations, unity power factor expression is found as:

$$L_d i_d^2 + L_q i_q^2 + i_d \lambda_m = 0 \tag{3.6}$$

3.4.3 Constant Stator Flux Control

Using this strategy, voltage is maintained low by limiting the magnitude of the flux linkage λ_s in the stator. By limiting the flux below the saturation point stator, iron saturation will not appear [1]. The magnitude of stator flux linkage vector λ_s is expressed below:

$$\lambda_s = \sqrt{\lambda_{sd}^2 + \lambda_{sq}^2} = \sqrt{(L_d i_d + \lambda_m)^2 + (L_q i_q)^2} \tag{3.7}$$

Where λ_{sd} is the d component of the stator flux linkage vector, λ_{sq} is the q axis of the stator flux linkage vector. From all the control properties presented above constant stator flux control has better steady state performance characteristic. The drawback appears when the torque capability is limited as a reaction of stator flux linkage limitation

3.4.4 Maximum torque per ampere control

In this control property i_d and i_q current are controlled and reluctance torque is used. For a certain electromagnetic torque the amplitude of the current reaches a minimum, and the efficiency of the motor can be increased.

Using the torque equation and differentiating in concordance to the torque angle α , a new expression for i_d and i_q can be found. The equations 3.8, 3.9, 3.10 are taken from [12], [13] and used to generate the MTPA waveforms and also the relationship between d and q currents and the corresponding torque.

$$T_e = \frac{3}{2} n_{pp} \cdot (\Psi_m \cdot i_{qs}) + \frac{3}{2} n_{pp} \cdot (L_d - L_q) \cdot i_{ds} i_{qs} \tag{3.8}$$

$$i_{ds} = \frac{-\Psi_m + \sqrt{\Psi_m^2 + 8(L_d - L_q)^2 \cdot I_s^2}}{4(L_d - L_q)} \tag{3.9}$$

$$i_{qs} = \sqrt{I_s^2 - I_{ds}^2} \tag{3.10}$$

This control property is complex but an important advantage of this control is the use of reluctance torques. For this purpose this control property is used in the simulation of the machine.

From above equations can be observed that flux linkage and the d and q axis inductances have an important influence on the MPTA curve. An M-file which can be seen in Appendix B.4 was created to obtain the above mentioned waveforms , which is similar from the work done in [13]. The parameters used are taken from table 2.1 and the current magnitude of I_s is set to 30[A].

In Fig 3.7 L_d and L_q are constant. This can influence the machine control since the parameters are varying when saturation effects are taken into consideration.

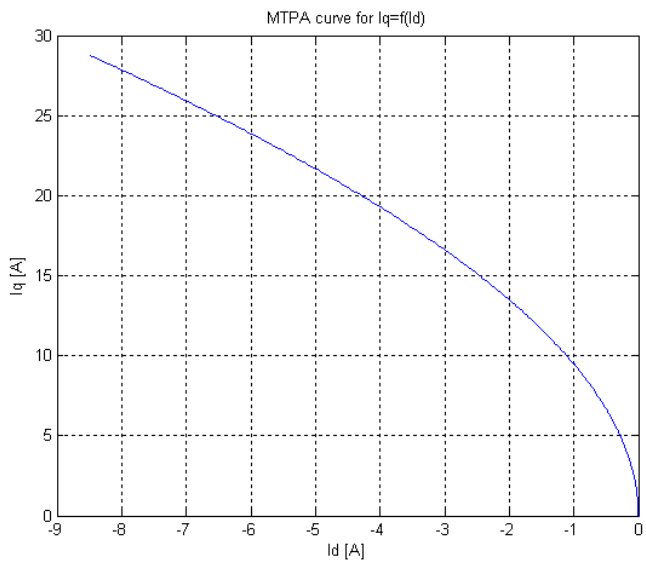

Figure 3.7: *MTPA curve for fixed L_d and L_q values*

In Fig 3.8 and Fig 3.9 the influence of the parameters can be seen when MPTA curve is plotted , by varying the L_d and L_q inductances.

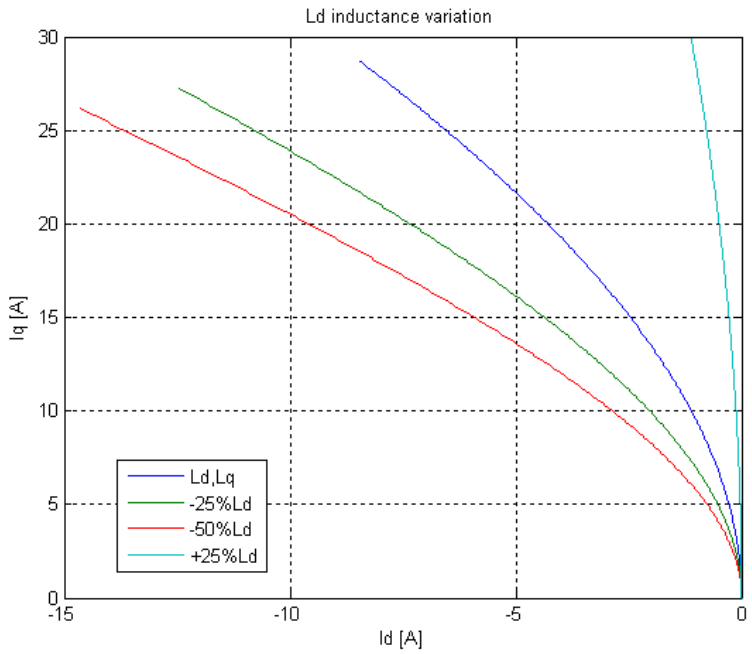

Figure 3.8: *MTPA curve for different L_d values*

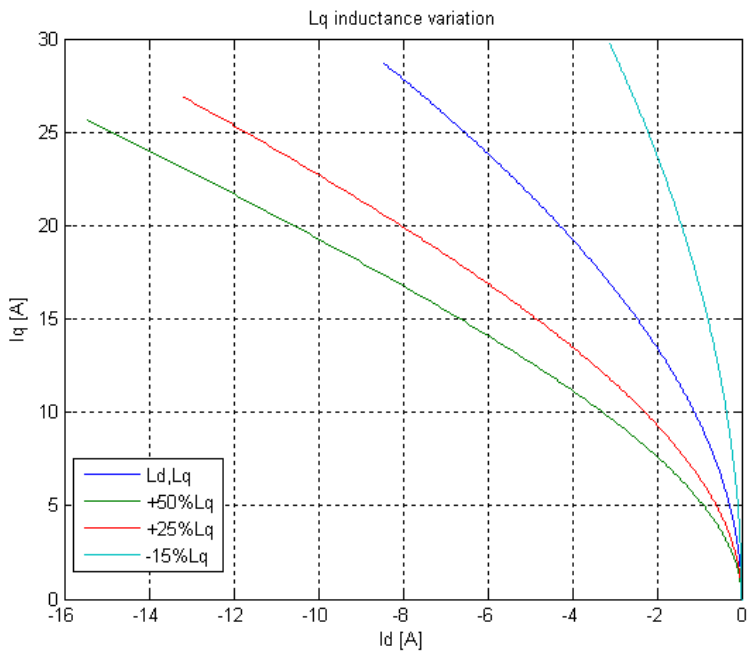

Figure 3.9: *MTPA curve for different L_q values*

In Fig 3.8 the L_d inductance is varied to -50%, -25% and +25% of the actual value. It can be noticed

that slope of the MPTA curve is decreasing by decreasing the L_d inductance. Regarding the currents , can be seen that I_d current is increasing and I_q current is decreasing . When the L_d inductance is increased the slope of MPTA curve is increasing. This means that I_d becomes smaller and the I_q is increased.
In conclusion the variation of L_d inductance is direct proportional with the slope of MPTA curve and I_q and inverse proportional to I_d.

In Fig 3.9 the L_q inductance is varied to +50%, +25% and -15% of the actual value. It can be observed that the slope of the curve is increased when L_q inductance is decreased. Al so it can be observed that I_q current is increasing while I_d current is decreasing. The slope of the curve is decreasing When the L_q inductance is increased. Regarding the currents the I_q current is decreasing while I_d current is increasing.

This means that L_q inductance variation is direct proportional with I_d and inverse proportional with slope of MPTA curve and I_q.

3.5 FOC Controlers design

In this section, the implementation of the currents and the speed controllers is presented. Two current controllers are used for the inner loop and one speed controller is used for the outer loop. The speed controller is slower than current controllers because the electrical system is faster than mechanical system.
The overall structure of the d and q-axis control loops is shown in Fig 3.10

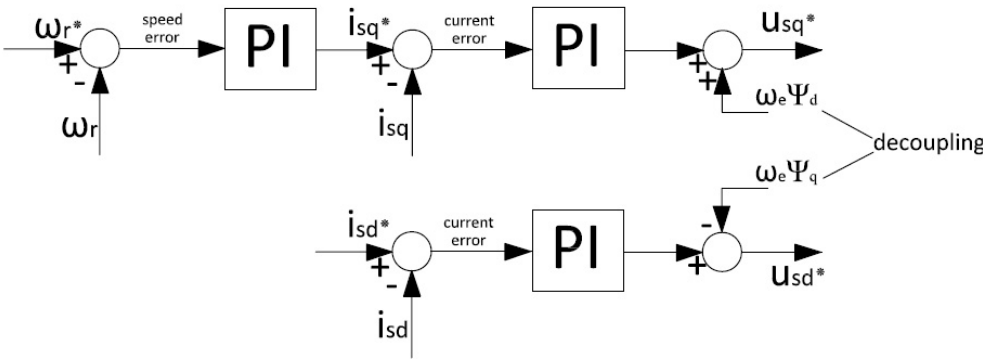

Figure 3.10: *Structure of FOC controllers [1]*

In the voltage equations presented in mathematical model, the dq-axis voltages are cross coupled. Due to this coupling the i_d and i_q currents cannot be controlled independently. The solution is to add and substract the decoupling terms to the current controllers in order to simplify and to improve the control accuracy.

After the decoupling has been performed, the voltage equations have the fallowing expresion:

$$u_{sd} = R_s i_{sd} + L_d \frac{di_{sd}}{dt} \tag{3.11}$$

$$u_{sq} = R_s i_{sq} + L_q \frac{di_{sq}}{dt} \tag{3.12}$$

In time domain, the equation for the PI controller used, applied to an error signal e(t) is:

$$u(t) = K_p \cdot e(t) + k_i \cdot \int_{t0}^{t} e(\tau) d\tau \tag{3.13}$$

where u(t) is the output signal, and k_p, k_i are the proportionality and the integration gains. The transfer function for the PI controller is the ratio between the output signal and error signal, as seen in below equation:

$$G(s) = \frac{U(s)}{E(s)} = k_p + \frac{k_i}{s} = k_p(\frac{s + \frac{1}{T}i}{s}) \tag{3.14}$$

where T_i is the ratio between k_p and k_i: $T_i = \frac{k_p}{k_i}$
In Fig 3.11 a general PI controller scheme can be seen:

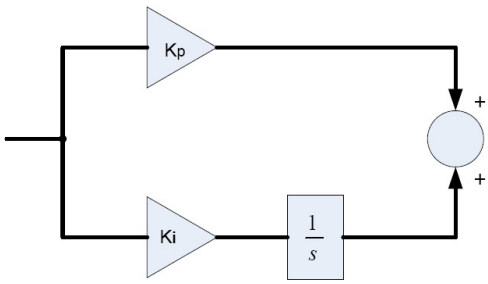

Figure 3.11: *PI block diagram*

3.5.1 q-axis current controller design

The i_{sq} loop is presented in Fig 3.12. The blocks in the current loop are:

- The PI current controller.
- Digital calculation delay. This has the form of a first order transfer function with the time constant T_s = 1/ f_s[ms], where f_s = 5[kHz] is the sampling frequency.
- The plant block.
- Digital to analog conversion delay. This is a first order transfer function with the time constant 0.5 T_s = 0.1[ms].

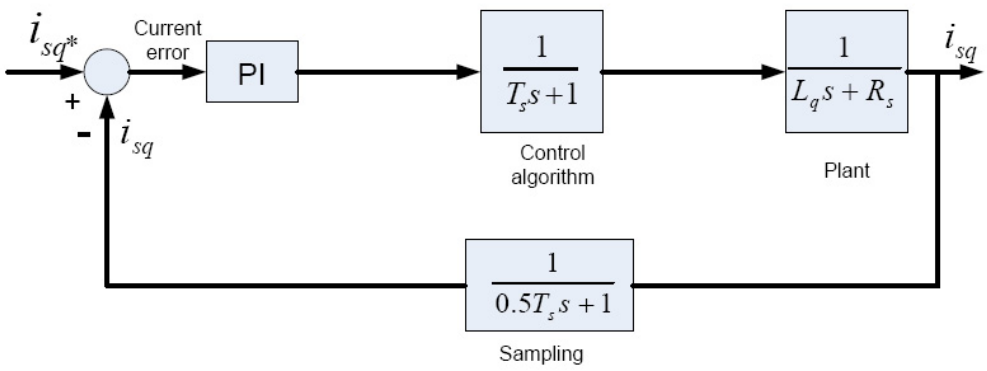

Figure 3.12: *Structure of q-axis current loop*

The transfer function of the plant is presented in equation 3.15.

$$G_p(s) = \frac{i_{sq}(s)}{u_{sq}(s)} = \frac{1}{R_s + sL_q} = \frac{1}{R_s}\frac{1}{1 + s\frac{L_q}{R_s}} = \frac{K}{1 + sT_q} \tag{3.15}$$

where K=$\frac{1}{R_s}$ and $\tau_q = \frac{L_q}{R_s} = 0.0373$[sec]. The open loop transfer function found can be seen in below equation:

$$G_{OL}(s) = k_{pi} \cdot \frac{1+T_i s}{T_i s} \cdot \frac{k}{\tau_s s+1} \cdot \frac{1}{T_s s+1} \cdot \frac{1}{1+0.5T_s s} \cdot \frac{1}{0.5T_{inv} s+1} \tag{3.16}$$

The zero of the controller is used to cancel the slowest pole of the transfer function, giving the equality:

$$T_i = \tau_q = \frac{L_q}{R_s} = 0.0373 \tag{3.17}$$

An equivalent time constant can be defined to simplify the transfer function:

$$T_{si} = 1.5T_s = 0.4[ms] \tag{3.18}$$

The new open loop transfer function becomes :

$$G_{OL}(s) = \frac{k_{pi}}{T_i s} K \frac{1}{T_{si} s+1} \tag{3.19}$$

In Fig 3.13 the root locus of the designed q-axis current controller can be seen.

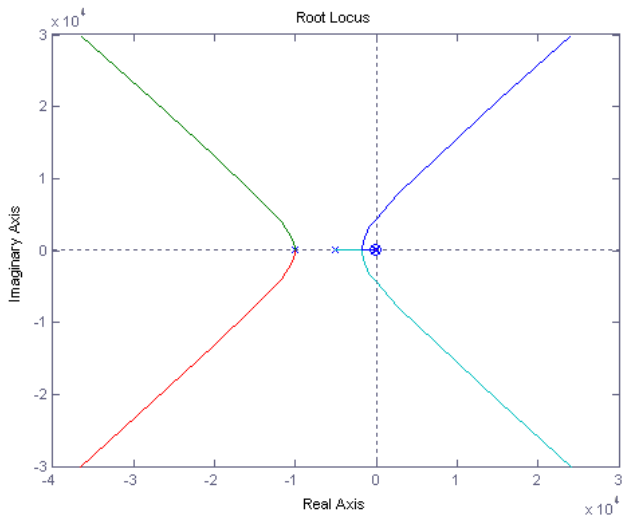

Figure 3.13: *q-axis current controller root locus*

The proportional gain of the PI controller, K_{pi_q} is calculated using the optimal modulus criterion, with the damping factor set to be $\zeta = \frac{\sqrt{2}}{2}$ [14]. The transfer function of a second order system is given in the following equation:

$$G_{OM}(s) = \frac{1}{2\tau s(\tau s+1)} \tag{3.20}$$

From the equation 3.20 and equation 3.19 results that : $k_{pi} = \frac{T_i R_s}{2T_s} = 5.1250$. The PI transfer function in s domain has the fallowing form: $G_c(s) = 5.1250 + \frac{137.5}{s}$

The Bode diagram of designed current controller is shown in Fig 3.14.

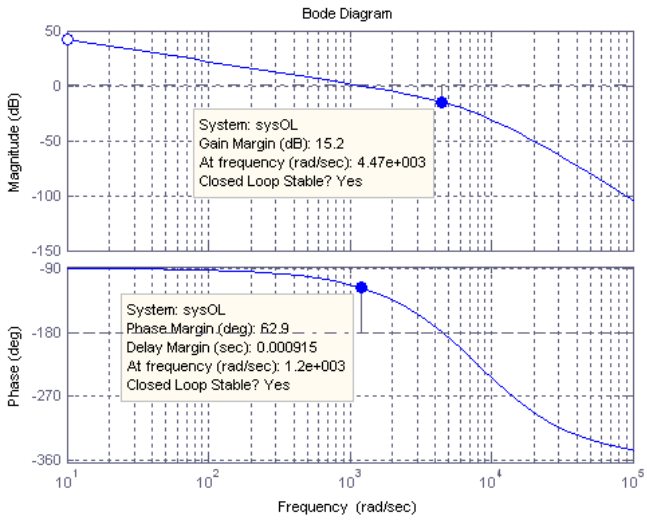

Figure 3.14: *q-axis current controller bode diagram*

The design of the I_{sq} PI controller leads to a gain margin of GM=15.2(dB) and a phase margin, PM=62,9(deg). As seen in the above figure the closed loop system is stable. To implement the control in real time, the controller is implemented also in z domain, as in equation 3.21.

$$PI(z) = 5.125 + \frac{135}{z-1} \tag{3.21}$$

Fig 3.15 presents the step response of the designed q-axis current controller in z domain. The settling time of the controller is t_s= 3.37[ms]. It can be seen while reaching steady state no overshoot occurs.

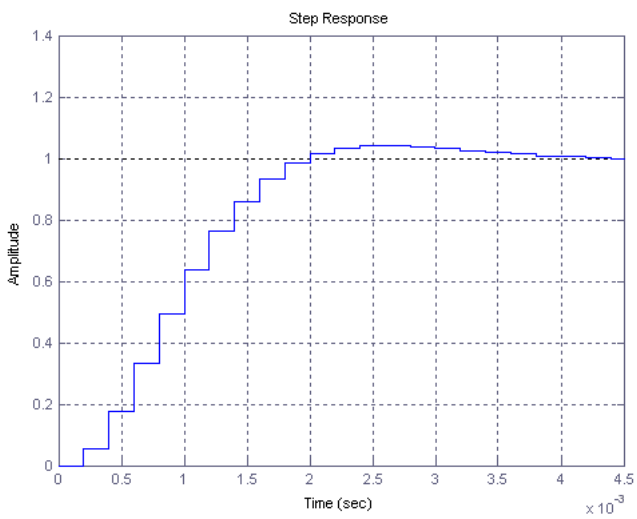

Figure 3.15: *q-axis current controller step response*

3.5.2 d-axis current controller design

The design steps made for q current controller are the same as for d current controller, in the continuous domain. All the delays are also the same, the only difference from the q current loop is the transfer function of the plant, which is different due to the L_d, L_q inductances difference.

In this case as seen in Fig 3.16 the plant transfer function is changed because $T_i = \tau_d = \frac{L_d}{R_s} = 0.0291$[sec]

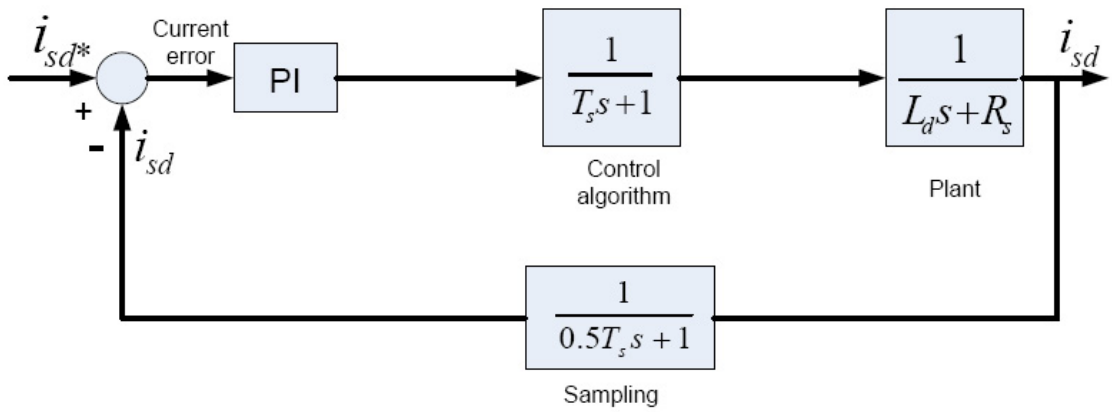

Figure 3.16: *Structure of d-axis current loop*

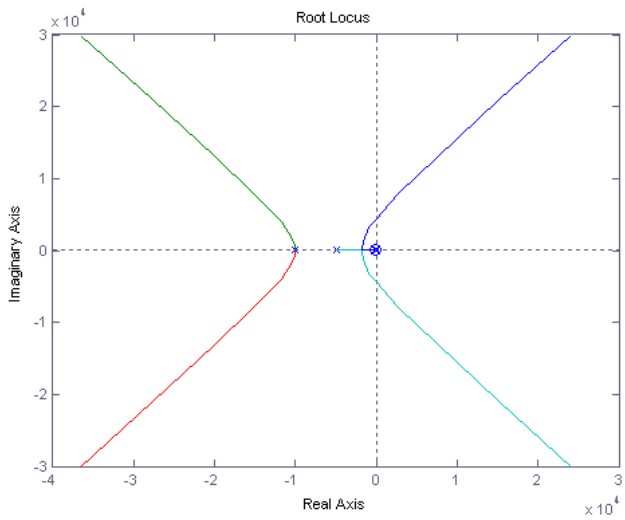

Figure 3.17: *d-axis current controller root locus*

From the open loop transfer function the proportional gain is obtained $k_{pi} = \frac{T_i R_s}{2T_{si}} = 4$. The root locus of d axis controller can be seen in Fig 3.17. The Bode diagram of designed current controller is shown in Fig 3.18, with gain margin of GM=15.2(dB) and a phase margin, PM=62,9(deg).

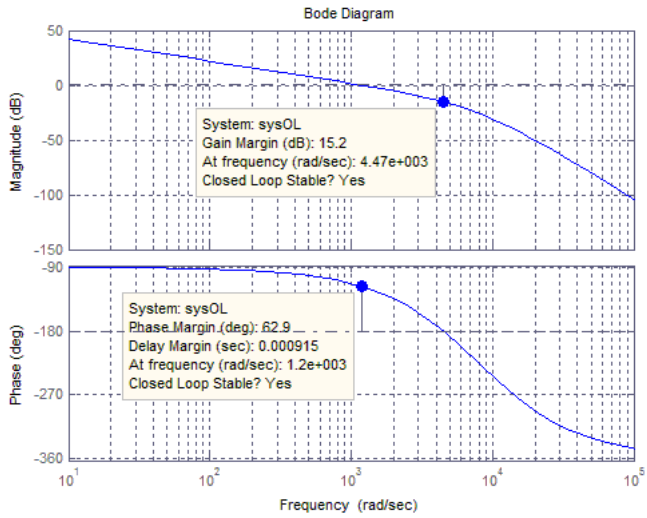

Figure 3.18: *d-axis current controller bode diagram*

The controller is implemented also in z domain, as in equation 3.22.

$$PI(z) = 0.07812 + \frac{135}{z-1} \tag{3.22}$$

In Fig 3.19 the step response of the designed d-axis current controller in z domain with settling time of t_s= 3.37[ms] is presented.

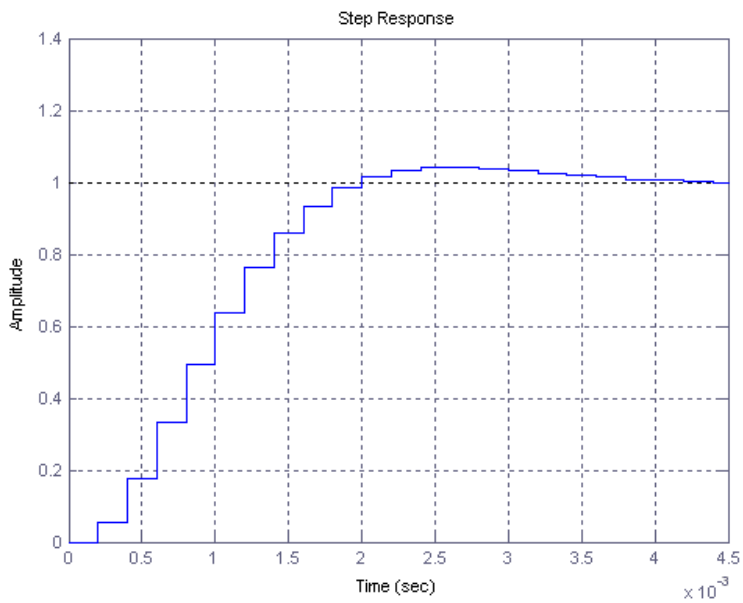

Figure 3.19: *d-axis current controller step response*

3.5.3 Speed controller

The structure of speed loop is presented in Fig 3.20, where T_e is the electromagnetic torque; T_L is the load torque; n_{pp} is the number of poles; ω_m is the mechanical speed.

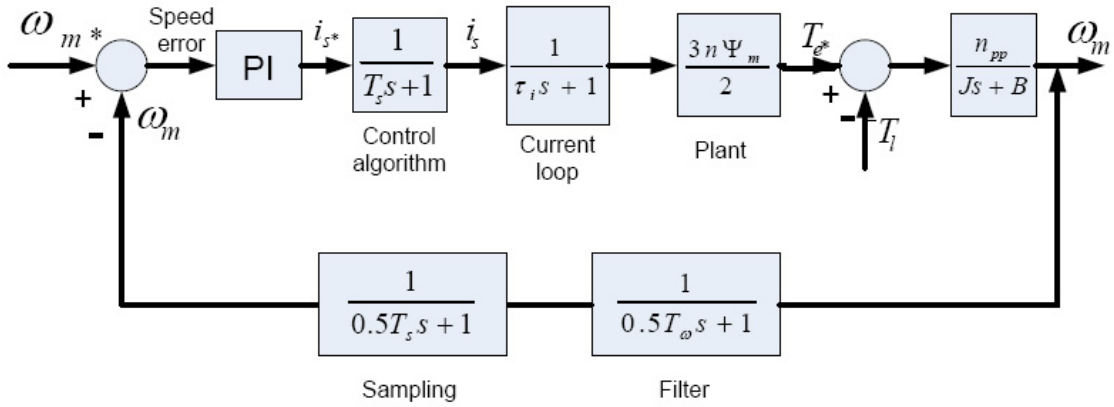

Figure 3.20: *Speed controller loop structure*

The blocks used in the above figure are :

- The PI current controller.
- Digital calculation delay. This has the form of a first order transfer function with the time constant T_s = 1/ f_s[ms], where f_s = 5[kHz] is the sampling frequency.
- The delay introduced by the current controller.
- The plant block.
- Digital to analog conversion delay. This is a first order transfer function with the time constant 0.5 T_s = 0.1[ms].
- The filter with the time constant T_{ω_c} = 1/ ω_c= 0.796[ms]

The transfer function of the PI speed controller is:

$$PI_\omega = k_p(\frac{1+T_\omega s}{T_\omega s}) \tag{3.23}$$

where k_p is the proportional gain and T_ω is the integrator time constant. From the mechanical equation the electrical speed is calculated. The viscous friction coefficient can be neglected since it has a small value. The electrical speed becomes:

$$\omega_{el} = \frac{n_{pp}}{Js}(T_e - T_l) \tag{3.24}$$

The open loop transfer function found is given in the below equation:

$$G_{OL}(s) = \frac{1}{1+0.5T_s s} \cdot \frac{1}{T_\omega s+1} \cdot k_p \cdot \frac{T_\omega s+1}{T_\omega s} \cdot \frac{1}{T_s s+1} \cdot \frac{1}{\tau_i s+1} \cdot \frac{3n\Psi_m}{2} \cdot \frac{n_{pp}}{Js} \tag{3.25}$$

An equivalent time constant is found in order to simplify the transfer function :

$$T_{s\omega} = 1.5T_s + \tau_i + T_{\omega c} = 0.0019 \tag{3.26}$$

From the open loop transfer function of the speed controller, presented in equation 3.27, the gains of the regulator can be found with the help of the optimum symmetric method.

$$G_{OL}(s) = \frac{\frac{n_{pp}K_T}{J}k_{p\omega}T_\omega s + \frac{nK_T}{J}k_{p\omega}}{s^2(T_{s\omega}T_\omega s + T_\omega)} \tag{3.27}$$

where K_t is the time constant of the current controllers: $K_t = (T_{ii} * R_s)/K_{pi} = 8[ms]$

The proportional and integral gains of speed controller found are shown in equation 3.28 and equation 3.29:

$$k_{p\omega} = \frac{1}{2k_1T_1} = \frac{1}{2\frac{n_{pp}K_T}{J}T_{s\omega}} = 0.0781 \tag{3.28}$$

$$T_\omega = 4T_1 = 4T_{s\omega} = 7.6 \tag{3.29}$$

The bode diagram can be seen in Fig 3.21, with gain margin of GM= 22.6(dB) and a phase margin, PM= 30.1(deg).

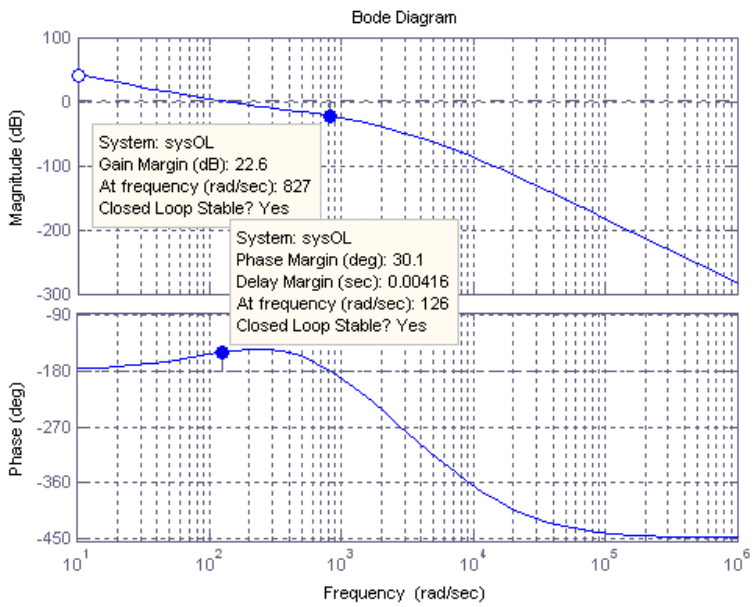

Figure 3.21: *speed controller bode diagram*

The speed controller is implemented also in z domain, as in equation 3.30.

$$PI(z) = 0.07812 + \frac{10.5}{z-1} \tag{3.30}$$

In Fig 3.22 the step response of the designed d-axis current controller in z domain with settling time of t_s= 0.0314[ms] is presented. In order to reduce the overshoot for the step response an antiwindup is introduced.

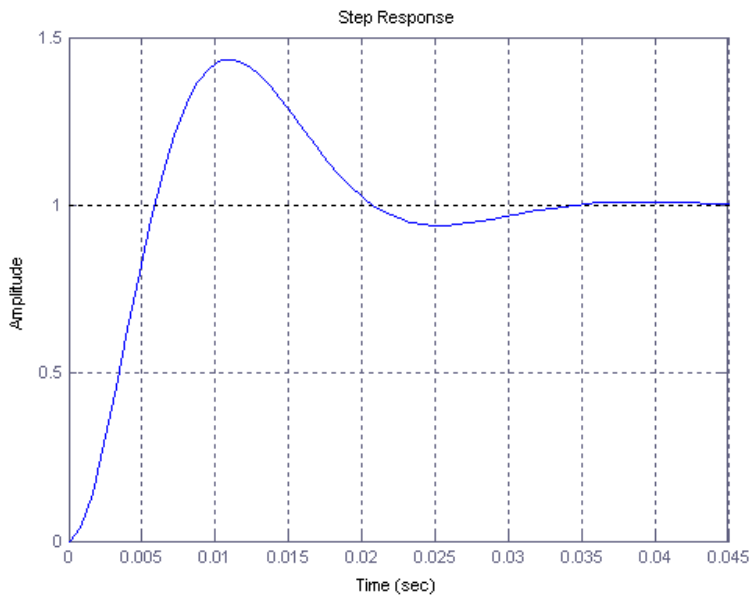

Figure 3.22: *speed controller step response*

3.5.4 Antiwindup structure

The voltages and currents represent the outputs of the designed controllers and are limited in order to prevent the appearance of overcurrent or overvoltage. Because of these outputs limitations, an anti-windup is necessary for the PI controllers, preventing delays in the PI response.

The structure of the PI with antiwind-up, for the current can be seen in the below picture, where K_a represent the antiwindup gain [10].

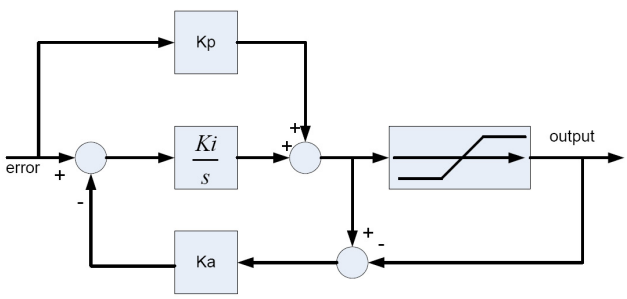

Figure 3.23: *Scheme of antiwindup structure*

When the signal becomes equal with the saturation level, the supplied error is integrated, increasing the output of the controller until the feedback of the plant exceeds the reference value and negative error appear in the PI input.

The effects of this phenomenon can be a large overshoots and if the signal saturation is persistent can damage the control.

To solve this problem an integrator antiwindup circuit is used to turns off the integral effect when the saturation occurs. Antiwindup gains are chosen in order to have the input of the integrator small, whenever the saturation occurs [10].

The gain used for controllers are: k_{aw}=100 for the speed controller and k_{ai}=r for the current controller.

3.6 Simulation results

In this section FOC strategy was tested. The values of the PI controllers used are the one calculated in the previous section. The electrical parameters implemented in the simulation are the one presented in Table 2.1, Section 2.6. All the simulations blocks are included in Apendix 1.

In order to test the simulations in real system all the calculation are done in discrete domain. The tests done are at no load, 50% loaded and at full load.

- Motor operation at no load and step in speed

  In this test the machine is started at no load and half of rated speed (n=2100[rpm]) followed by another step of 2100[rpm] supplied after 1.5 seconds.
  In the Fig 3.24 can be seen that the measured speed is following the reference speed with good accuracy.

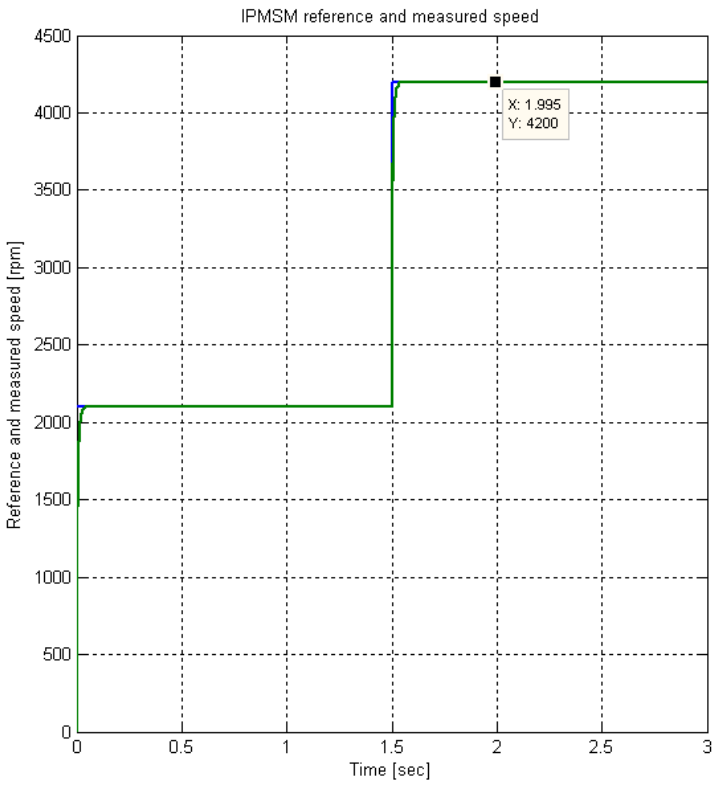

Figure 3.24: *The reference and measured speed response at no load*

In Fig 3.25 the d and q currents are presented. Because of the control strategy I_d current is zero. When the speed step is applied at 1.5 seconds the I_q current increases until the limited value of 43[A].
Since the load torque is zero and the machine is running in speed mode the dq currents are stabilized to zero.

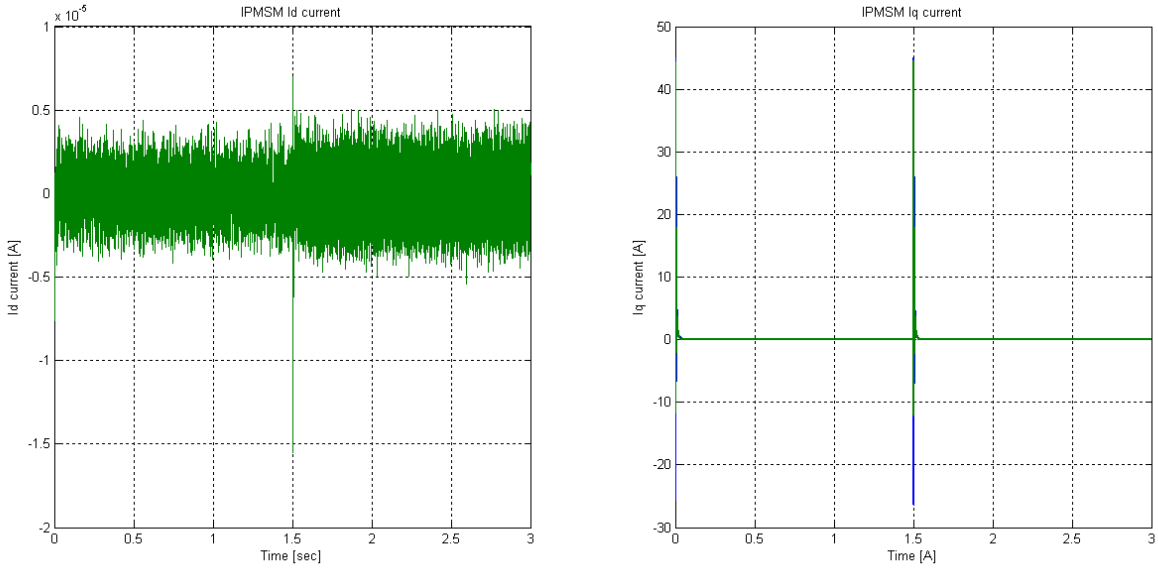

(a) Id current response

(b) Iq current response

Figure 3.25: *Reference and measured currents at no load*

Stator currents and voltages are shown in Fig 3.26. The voltage amplitude at half of the rated speed is 50[V] and 105[V] after 1.5 seconds when the rated speed is reached. From Fig 3.26a can be seen that the stator current is zero since the load torque is 0. At 1.5 seconds in transient period it is observed that the current is increased to the limited value due to the increase in speed.

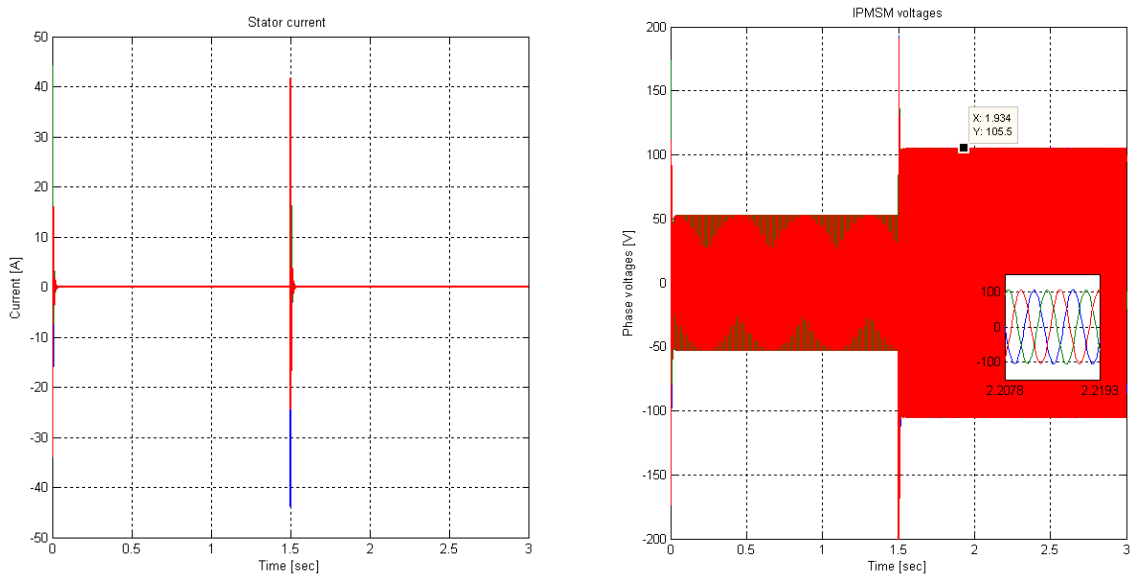

(a) Current response

(b) Voltage response

Figure 3.26: *Stator current and voltage at no load and step in speed*

- Motor operation at 50% rated torque and step in speed until nominal speed

  For this test the same procedure as for the test one was followed. The machine was loaded with 7.5[Nm] and started at a reference speed of 2100[rpm]. At second 1.5 another speed step of 2100[rpm] is supplied to the machine. Reaching the nominal speed, the measured speed follows the reference speed with a good accuracy and without overshoots. The response of the speed when a load is applied is slower than in the case were the load is zero.

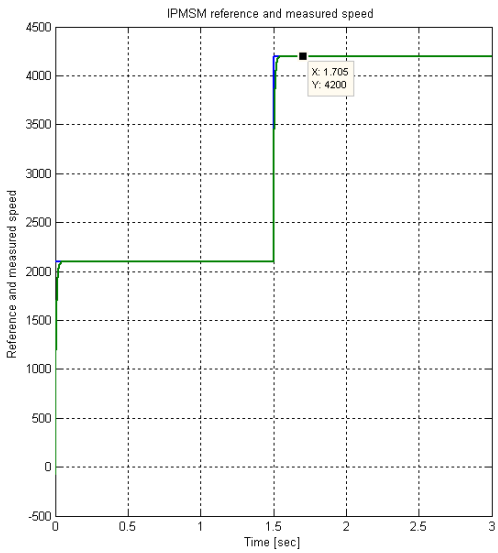

Figure 3.27: *The reference and measured speed response loaded at 7.5 [Nm]*

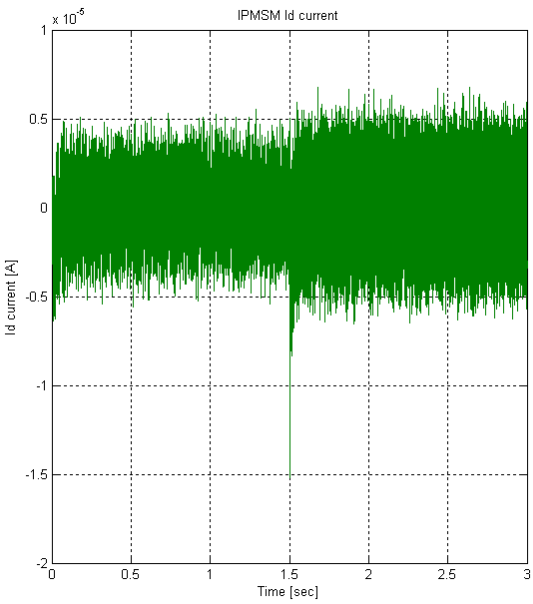

(a) Id current response

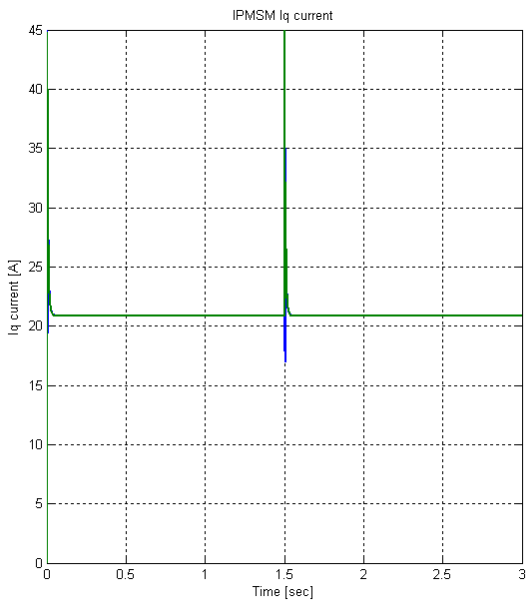

(b) Iq current response

Figure 3.28: *Reference and measured currents loaded at 7.5[Nm]*

In Fig 3.28 the dq currents and the reference currents are presented, where I_d is zero and I_q is limited to 45[A]. The stator current and voltages are shown in Fig 3.29, with values of 20[A] for the current and 155[V] for the voltage at half of the rated speed.

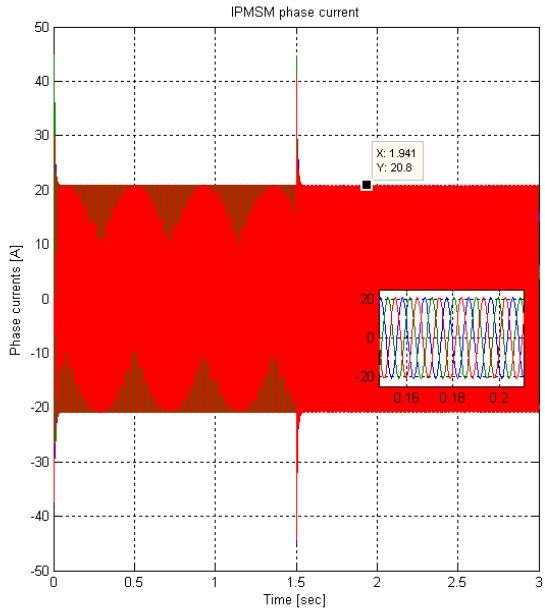

(a) Current response

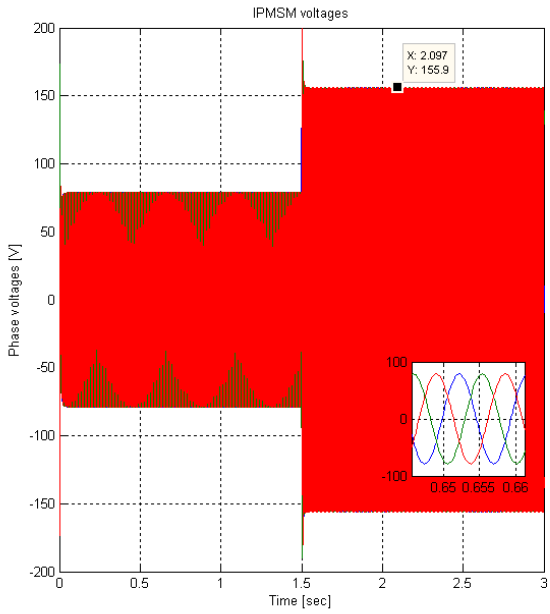

(b) Voltage response

Figure 3.29: *Stator current and voltage loaded at 7.5[Nm]*

- Motor operation at full rated torque and step in speed until nominal speed

In the last test the machine is running at nominal speed and also loaded at nominal torque. In Fig 3.30 the reference and measured speed is presented. The machine is started at 2100[rpm] which is half of the rated speed as mentioned above. At 0.5 seconds a load torque of 7.5[Nm] is applied , followed by a step to rated speed and at 2 seconds a step to nominal load torque.

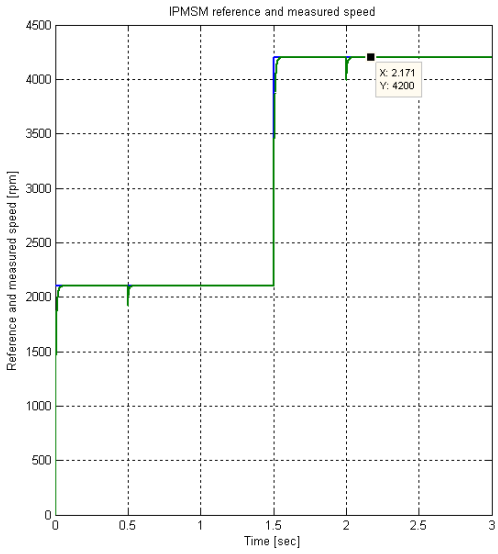

Figure 3.30: *The reference and measured speed increases until nominal speed and load torque are reached*

In Fig 3.31 the dq currents are presented. It can be observed that the measured currents are fallowing with good accuracy the reference currents for the changes made in the system.. The I_q value obtained is almost 42[A] while I_d is zero.

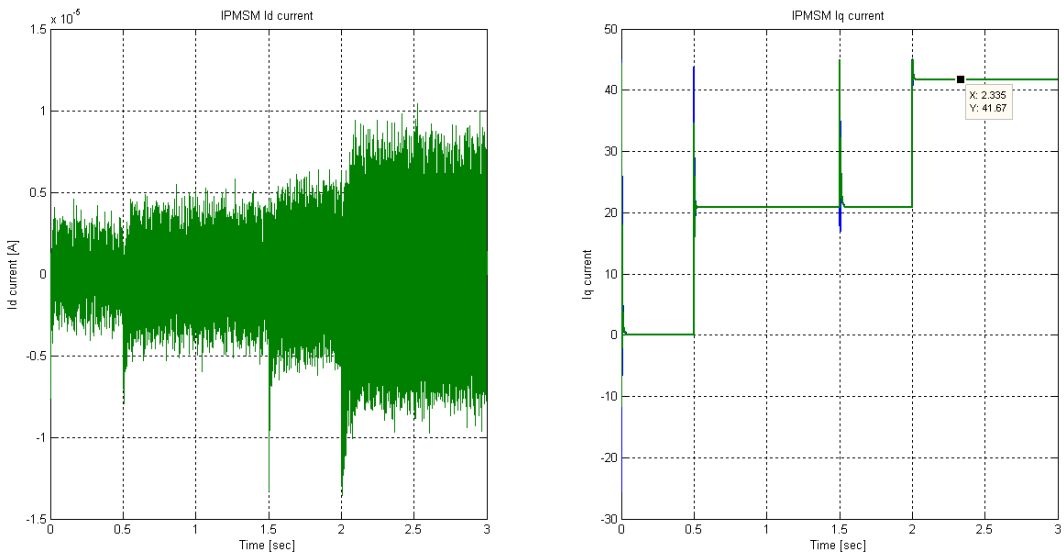

(a) Id current response

(b) Iq current response

Figure 3.31: *Reference and measured currents from zero to nominal load torque*

Fig 3.32 shows the stator current and voltage waveform for the same conditions explained above. At rated speed and load torque the values obtained for the current is almost 42[A] and for voltages is 250[V].

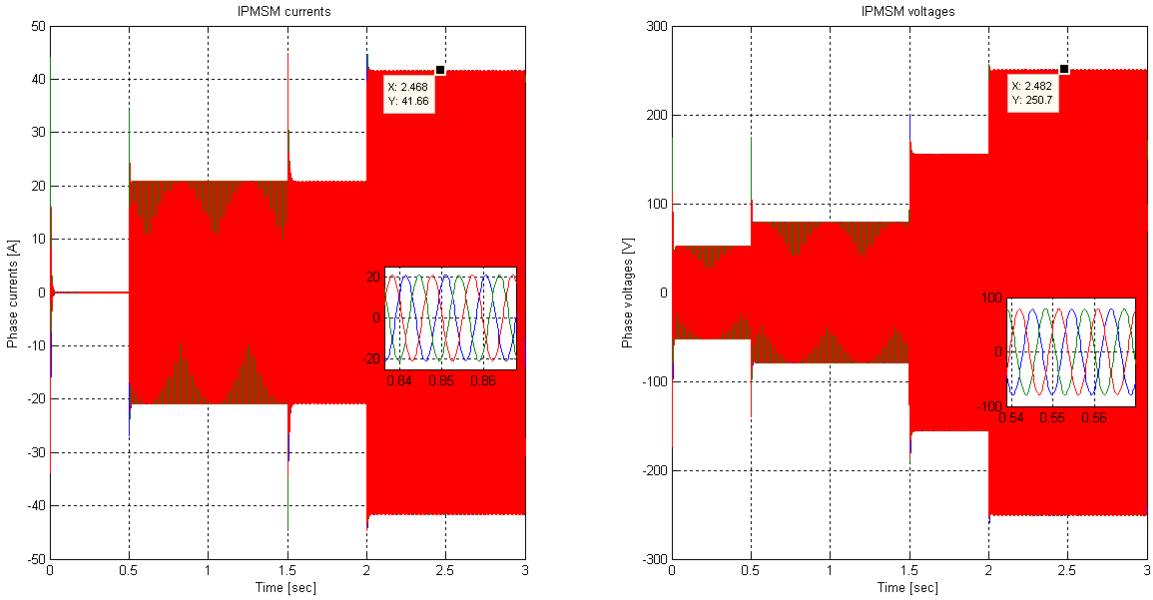

(a) Current response

(b) Voltage response

Figure 3.32: *Stator current and voltage from zero to nominal load torque, starting from half to nominal rated speed*

In Fig 3.33 the electromagnetic torque can be seen. The electromagnetic torque shows good behavior at the steps in speed and in load torque. When the rated torque and nominal speed is applied the value obtained for the electromagnetic torque is 15[Nm] as given in Table 2.1.

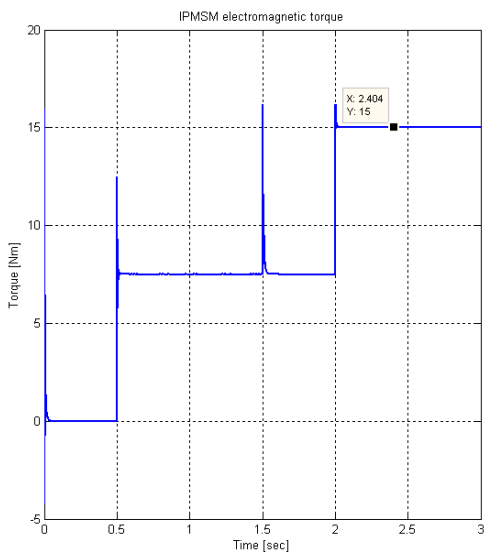

Figure 3.33: *Electromagnetic torque response at nominal speed and load torque*

3.7 Steady-State simulation

The steady state simulation of IPMSM with inductances variations was made since all the inductance measurements are done under static tests.

There are different ways to include the saturation effect in simulation, by FEM simulation or by using mathematical approach . One method, is to obtain the desired inductance values by knowing the slope and the maximum and minimum values for current and inductance.

Firstly, an inductance saturation level is defined as in equation 3.31 which is the weight of a saturated inductance L_s and the minimal inductance value L_{min}.

$$IndSatLevel = \frac{L_{min}}{L_s}\varepsilon[0,1] \tag{3.31}$$

If the maximum and minimum currents I_{max}, I_{min} and the maximum and minimum inductance L_{max}, L_{min} are known the inductance saturation profile slope m can be calculated as in equation 3.33.

$$m = \frac{L_{max} - L_{min}}{I_{max} - I_{min}} \tag{3.32}$$

If the slope and current amplitude are known the inductance value may be calculated as follows:

$$L_x = L_{max} - m(I_{min} - I_x) \tag{3.33}$$

Where L_x can be L_d or L_q and I_x is the actual current value.

Another mathematical approach is done by using two saturation factors S_d and S_q. The saturated values of the machine mutual reactance in d and q axes S_{mds} and S_{mqs} can be obtained by modifying their unsaturated values S_{md} and S_{mq} like in equations 3.34 and 3.35. More information can be found in [16].

$$X_{mds} = S_d \cdot X_{md} \tag{3.34}$$

$$X_{mqs} = S_q \cdot X_{mq} \tag{3.35}$$

A single saturation factor approach can also be used as in [17] using a saliency factor. The drawback is that the saturation factor is considered constant and in this case the d and q axis saturate to the same degree.

Another way for including saturation in IPMSM is to use look up tables as in [18]. In linear case the currents are deduced from the flux. For saturated case a high coupling between the two axis appear so the flux or the inductances are determined with contribution of I_d and I_q. In this way the cross saturation is included.

In Fig 3.34 a steady state model with saturation included is made using two look up tables as in [18]. Using Matlab commands *polyfit* and *polyval* the inductances are solved offline for different currents value, and the look-up-tables are populated with the obtained data.

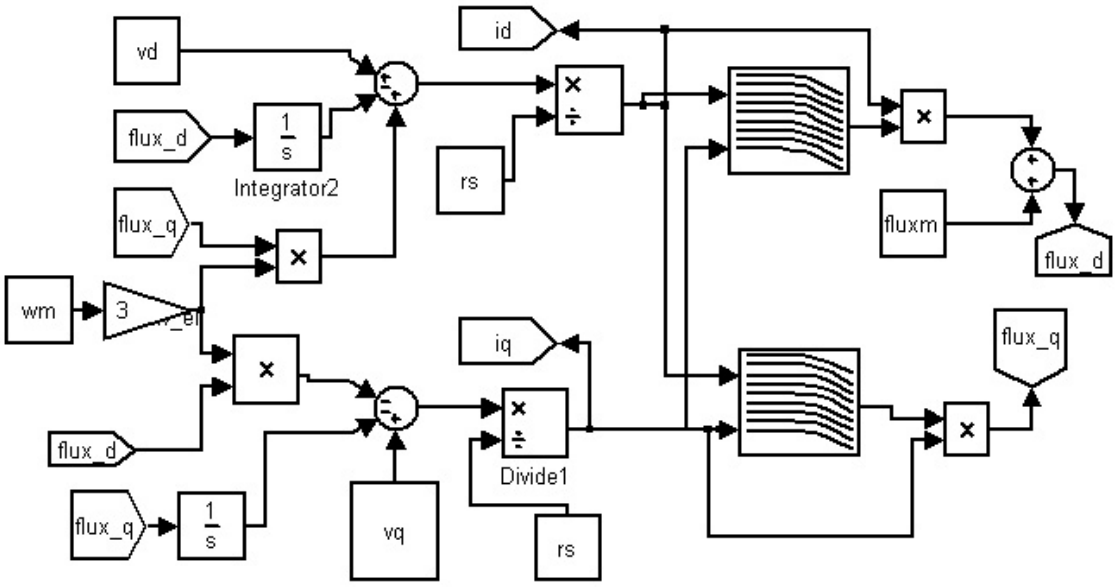

Figure 3.34: *Steady state simulation with inductance variation included*

In Fig 3.35 the L_d variation in function of I_d and I_q currents can be seen. It can be observed that for I_q=0 the L_d has the maximum value as in Table 2.1. It can be stated that L_d inductance is decreasing if I_q is increased. For maximum I_q the L_d inductance has a minimum value because of the cross saturation effect.

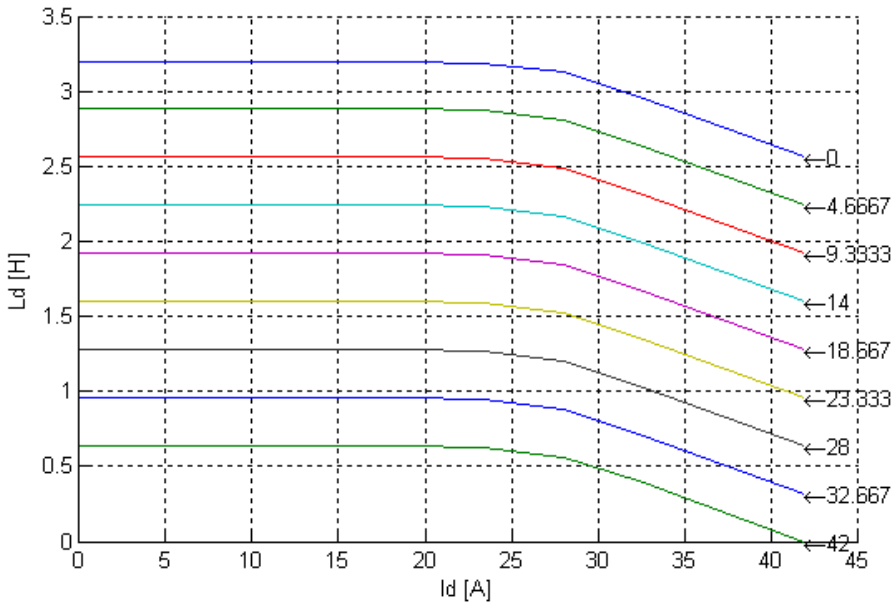

Figure 3.35: *L_d variation in function of I_d and I_q*

In Fig 3.33 a 3D plot is made in order to see the saturation level. It can be seen that for higher current the inductace is lower.

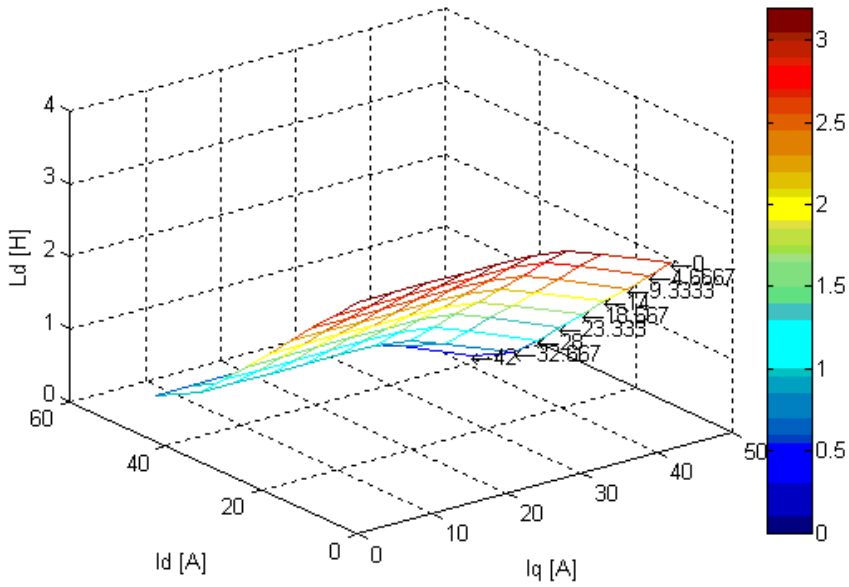

Figure 3.36: *L_d saturation in function of I_d and I_q*

In Fig 3.37 the L_q variation in function of I_d and I_q currents can be observed. Because of the cross saturation effect the L_q inductance is decreasing if I_d is increased. For maximum I_d current the L_d has the lowest value.

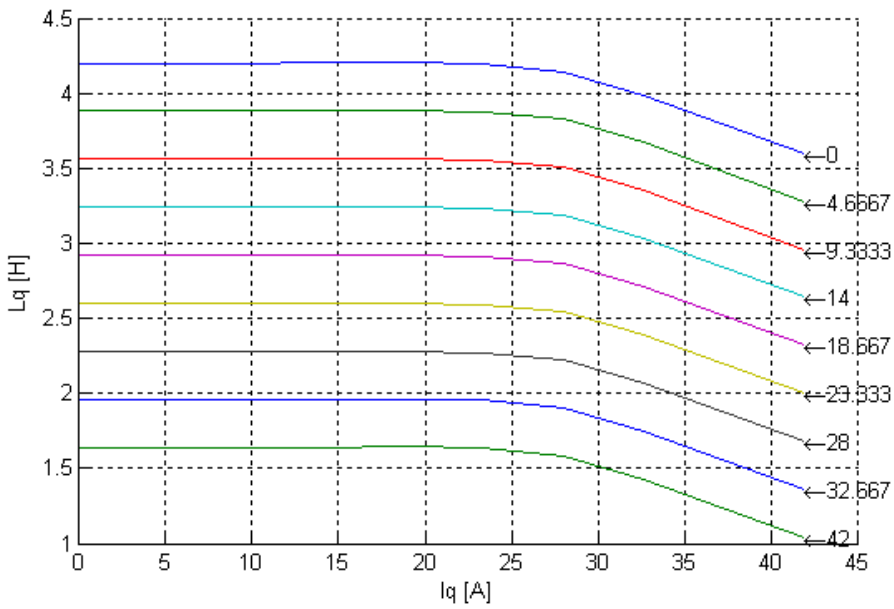

Figure 3.37: *L_q variation in function of I_d and I_q*

In Fig 3.38 a 3D plot was done to see the saturation level for L_q inductance. The same behavior as for L_d inductance can be observed , the only difference is the current which affect the L_q inductance. In this case the saturation effect appear when I_d is incresed.

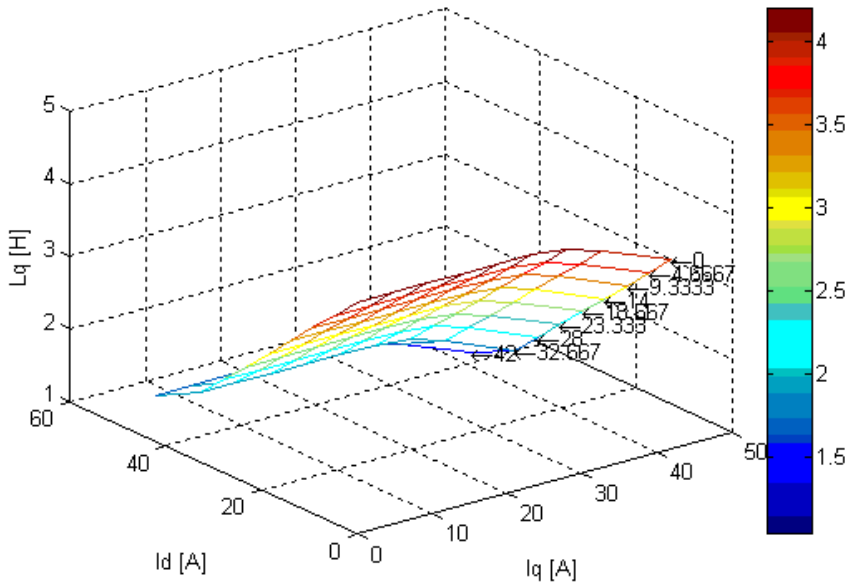

Figure 3.38: *L_q saturation in function of I_d and I_q*

Chapter 4

Experimental tests and results

4.1 Torque calibration

The purpose of this chapter is to present the laboratory work. The chapter begins with a presentation of the torque and inductance measurements procedures, followed by a description of the main components of the test setup. At the end of each measurement, the laboratory results are presented and commented.

In order to make a proper measurement, a calibration of torque was done because deformation of the shaft can appear during experiments.

The setup used for this experiment can be seen in Fig 4.1. In the setup an IPMSM and step motor are used. The experiment was done in steady state and as seen in the figure below an arm length was added to the shaft.

Weights were added in different steps from 0 to 3.9 [Kg] on the each side of the arm length. Knowing the weights added, the arm length and the gravitational force (G=9.8[Nm]), the torque can be calculated and compared with the measured one.

Figure 4.1: *Setup used for torque calibration*

In Fig 4.2 the calculated and measured torque as a function of the weights added can be seen. The two waveforms are linear and almost identical. Also it can be observed that the torque is direct proportional with the weight.

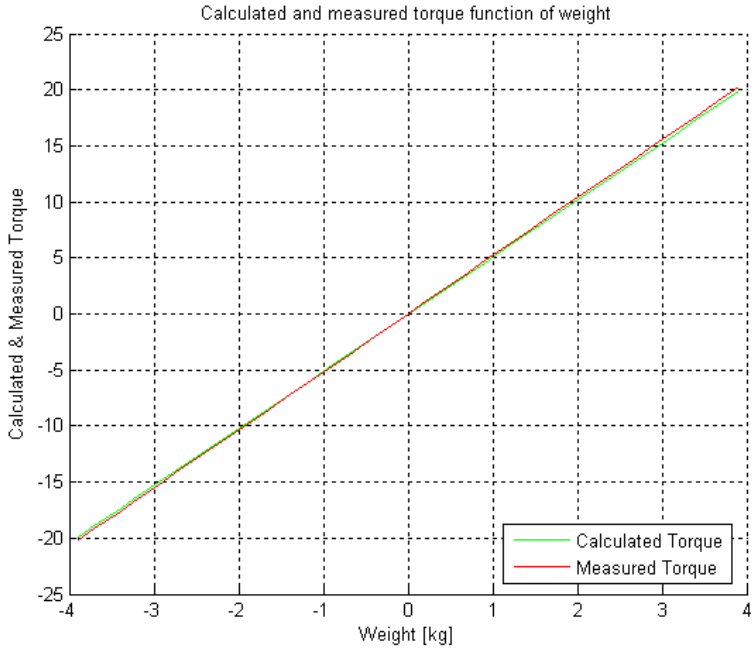

Figure 4.2: *Calculated and measured torque in function of weight*

4.2 Torque measurement

In this experiment the torque was measured using a mathematical approach. First different values for d and q currents are chosen. This means that the current on phase a (I_a) and rotor position θ_r can be calculated for each d and q currents pair.
In equations 4.1 and 4.2 the abc and dq current formula in vector form is expressed.

$$\bar{i}_{abc} = \frac{2}{3}(i_a + i_b e^{j\frac{2\pi}{3}} + i_c e^{-j\frac{2\pi}{3}}) \tag{4.1}$$

$$\bar{i}_{dq} = (i_d + j i_q)e^{j\theta_r} \tag{4.2}$$

In equation 4.3 dq currents are expressed as a function of abc current and rotor angle θ_r in vector form.

$$\bar{i}_{dq} = \bar{i}_{abc} \cdot e^{-j\theta_r} \tag{4.3}$$

Next a detailed expression for d and q currents is presented in equation 4.4 and 4.5.

$$i_d = \frac{2}{3}(i_a \cdot cos(\theta_r) + i_b \cdot cos(\theta_r - \frac{2\pi}{3}) + i_c \cdot cos(\theta_r + \frac{2\pi}{3})) \tag{4.4}$$

$$i_q = \frac{2}{3}(-i_a \cdot sin(\theta_r) - i_b \cdot sin(\theta_r - \frac{2\pi}{3}) - i_c \cdot sin(\theta_r + \frac{2\pi}{3})) \tag{4.5}$$

In Fig 4.3 it can be seen that two phases are short-circuited in order to make the following assumption:

$$i_a = -2i_b = -2i_c$$

By using this approach the current on phase a (i_a) is used to determine individually the i_d and i_q currents. Also only a DC source is needed for the experiment.

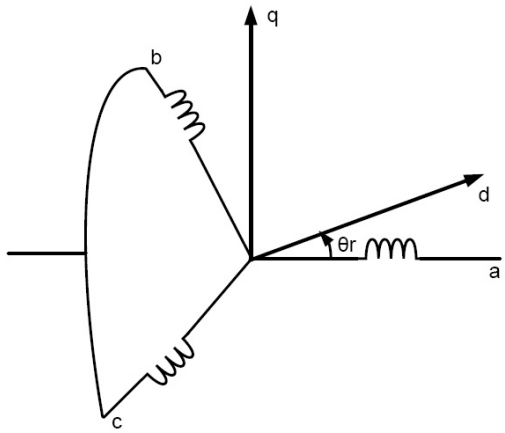

Figure 4.3: *IPMSM windings conections*

This leads to a new formula for d and q currents which depends only on the current of phase a (I_a) and rotor angle.

$$i_d = -\frac{2}{3}(i_a \cdot cos(\theta_r) - \frac{1}{2}i_a \cdot cos(\theta_r - \frac{2\pi}{3}) - \frac{1}{2}i_a \cdot cos(\theta_r + \frac{2\pi}{3})) \tag{4.6}$$

$$i_d = \frac{2}{3}(i_a \cdot cos(\theta_r) - \frac{1}{2} \cdot i_a cos(\theta_r) = \frac{2}{3}i_a\frac{3}{2}cos(\theta_r) = i_a \cdot cos(\theta_r) \tag{4.7}$$

Similar procedure is applyed for I_q and the final expresion is:

$$i_q = -\frac{2}{3}(i_a \cdot sin(\theta_r) + \frac{1}{2}i_a \cdot sin(\theta_r)) = -i_a \cdot sin(\theta_r) \tag{4.8}$$

If the d and q currents are known, the rotor angle and the phase current can be obtained as in equations 4.9 and 4.10.

$$i_a = \sqrt{i_d^2 + i_q^2} \tag{4.9}$$

$$\theta_r = tg^{-1}(\frac{-i_q}{i_d}) \tag{4.10}$$

In Fig 4.4 the setup used for this measurement can be seen. Using the PC program, the step motor is controlled in order to rotate the shaft with a desired angle calculated like as in equation 4.10. The DC source is used to supply the IPMSM motor with the desired current value as in equation 4.9.

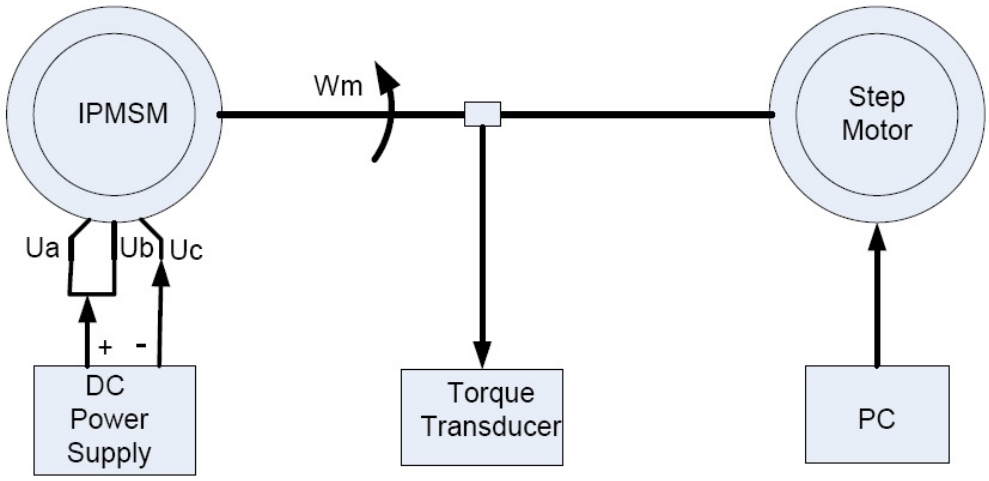

Figure 4.4: *IPMSM windings conections*

Since the right values for current and angle are set in this manner for all the measurements, the torque can be measured using a torque transducer. All the data measured are included in a mat file included in the CD and attached to the report.

The calculated torque presented as in equation 4.11 expressed as a function of I_d and I_q current can be seen in Fig 4.5. It can be observed that for negative values of the I_d current the torque is increasing and for positive values of I_d current the torque is decreasing. All the equations used for calculating the torque are included in Apendix B.2.

$$T_{cal} = \frac{3}{2} \cdot n_{pp}(\psi_m I_q + (L_d - L_q) \cdot I_q I_d) \tag{4.11}$$

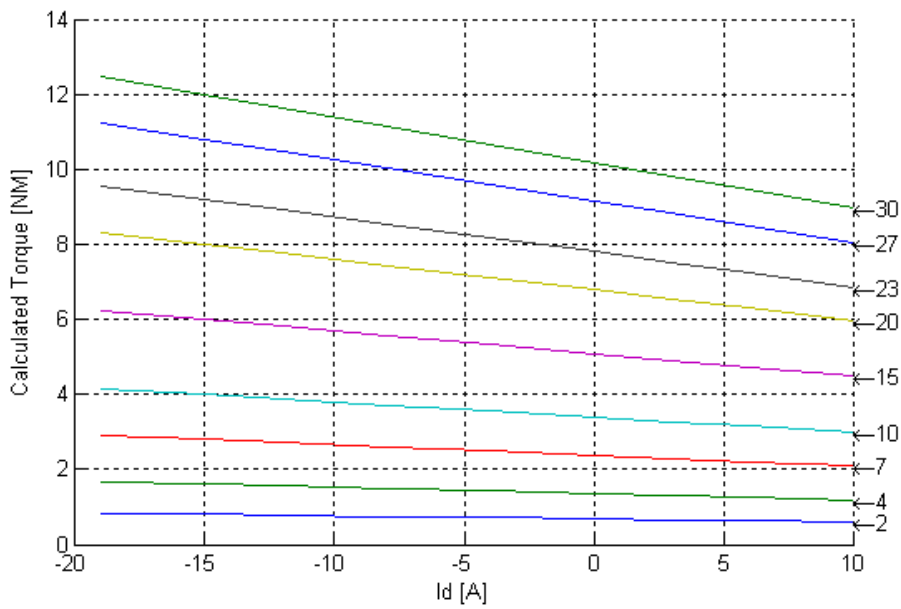

Figure 4.5: *Calculated Torque for different I_d and I_q*

In Fig 4.6 the measured torque as a function of I_d and I_q currents can be observed. The behavior of the measured torque is similar with the calculated one, the only difference is between -10 and 0 Ampere when torque is starting to increase. This phenomenon may be a consequence of the cross-coupling.

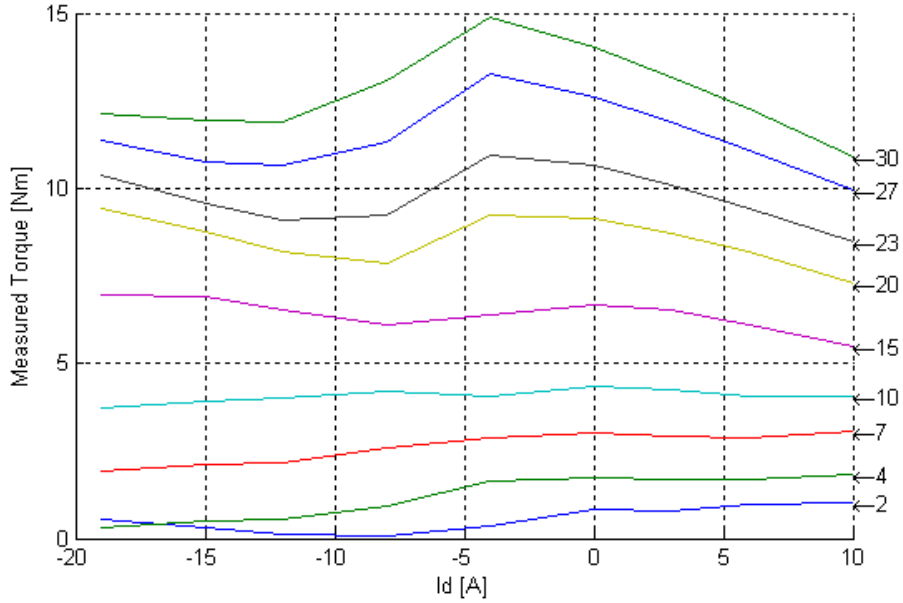

Figure 4.6: *Measured Torque for different I_d and I_q*

The calculated torque in function of I_q and I_d currents is presented in Fig 4.7. When I_q has smaller values the torque reaches high values, and when I_q increases the torque starts to decrease.

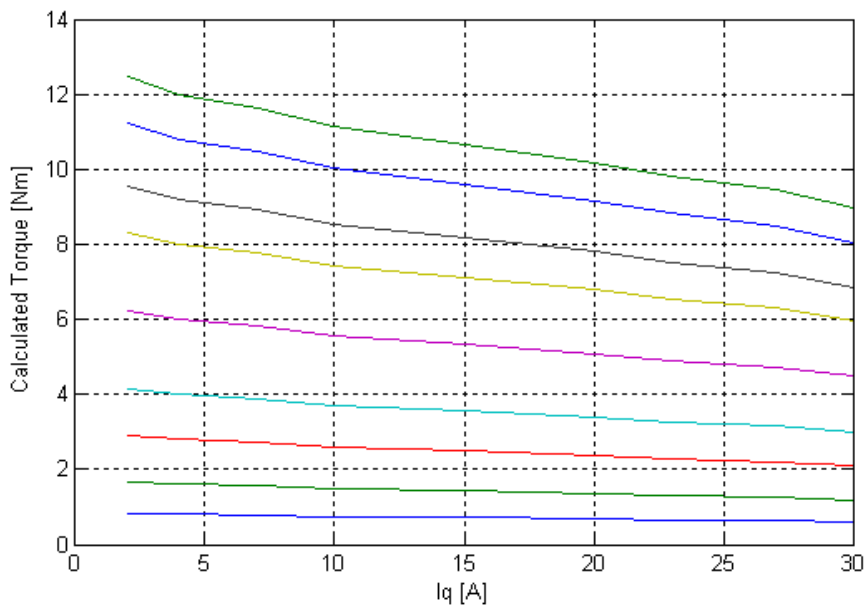

Figure 4.7: *Calculated Torque for different I_q and I_d*

The measured torque as a function of I_q and I_d current can be observed in Fig 4.8. From Fig 4.6 it can be observed that until the current reaches almost 10[A] the electromagnetic torque has the same value as in calculated torque. From 10[A] to 20[A] an increase in torque is observed. This may be a consequence of the crosscoupling.

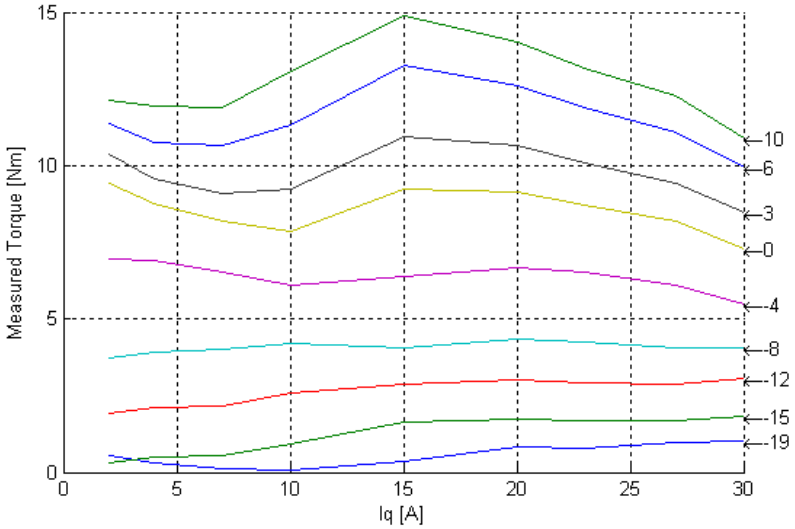

Figure 4.8: *Measured Torque for different I_q and I_d*

In order to see if the calculated and measured torque are correct, a comparison between the results obtained above and the torque expressed as a function of I_d and I_q currents is done. The data that are used for the comparision are presented in Fig 4.9 and are taken from [15] where a similar topic was studied for a PHD Thesis. It can be observed that a high torque appears for negative values of I_q and for positive values of I_d due to cross saturation apearence.

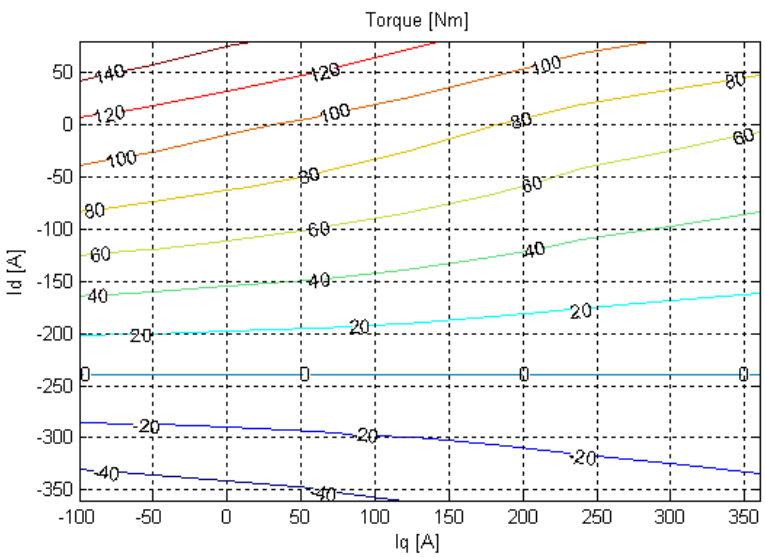

Figure 4.9: *Torque function of I_d, I_q*

In Fig 4.10 and Fig 4.11 the calculated and measured torque are plotted in a 3D waveform as a function

of I_d and I_q. It can be stated that for positive I_d values and lower I_q values the torque is maximum for the results presented in Fig 4.9.

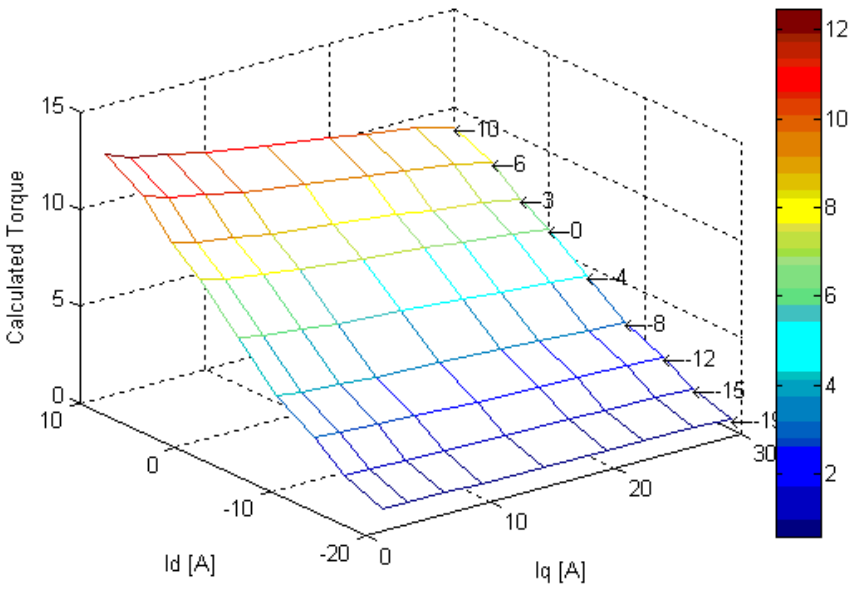

Figure 4.10: *Calculated torque function of I_d, I_q*

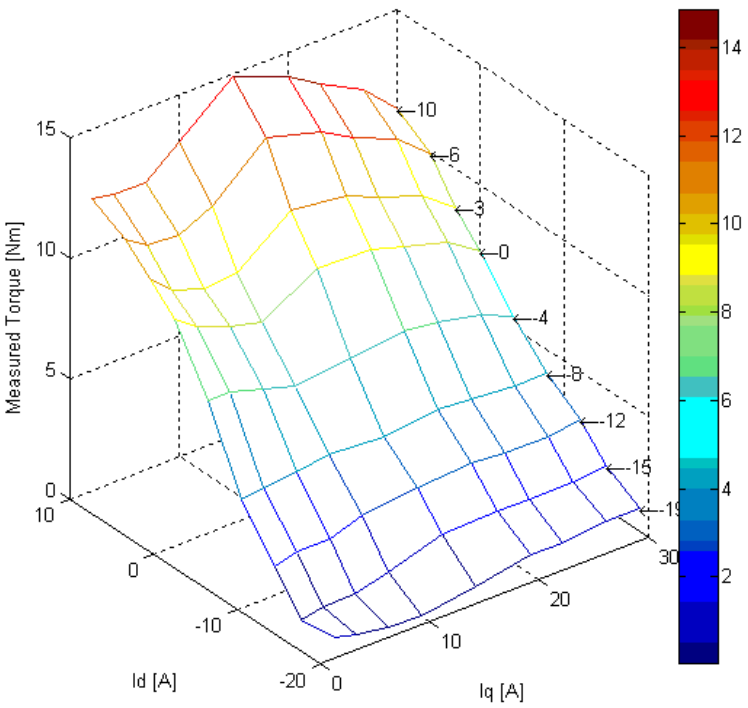

Figure 4.11: *Measured torque function of I_d, I_q*

4.3 Inductance measurement

In this section the procedure for inductance measurement is presented. First the mathematical approach is described. Starting from Fig 4.12 the reference frame transformation from dq to abc and from abc to dq can be found as in equation 4.12 and 4.13.

Using the following mathematical approach presented below only a DC source is used for the experiment. Since I_d and I_q currents are substituted in the current on phase a (i_a), the L_d L_q inductance can be determined individualy.

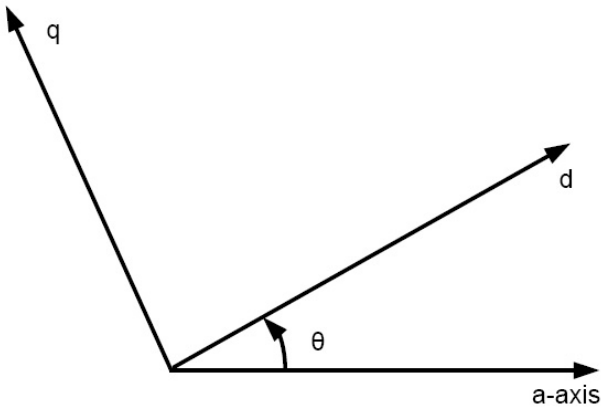

Figure 4.12: *Reference frame diagram*

$$\begin{bmatrix} f_d \\ f_q \\ f_0 \end{bmatrix} = \frac{2}{3} \cdot \begin{bmatrix} cos(\theta) & cos(\theta - \frac{2\pi}{3}) & cos(\theta + \frac{2\pi}{3}) \\ -sin(\theta) & -sin(\theta - \frac{2\pi}{3}) & -sin(\theta + \frac{2\pi}{3}) \\ \frac{1}{2} & \frac{1}{2} & \frac{1}{2} \end{bmatrix} \cdot \begin{bmatrix} f_a \\ f_b \\ f_c \end{bmatrix} \tag{4.12}$$

$$\begin{bmatrix} f_a \\ f_b \\ f_c \end{bmatrix} = \frac{2}{3} \cdot \begin{bmatrix} cos(\theta) & -sin(\theta) & 1 \\ cos(\theta - \frac{2\pi}{3}) & -sin(\theta - \frac{2\pi}{3}) & 1 \\ cos(\theta + \frac{2\pi}{3}) & -sin(\theta + \frac{2\pi}{3}) & 1 \end{bmatrix} \cdot \begin{bmatrix} f_d \\ f_q \\ f_0 \end{bmatrix} \tag{4.13}$$

Shortcircuiting two phases of the machine as presented in Fig 4.13 and using the neutral point the line to line voltage can be formulated as V_{ab}= V_{aN}- V_{bN}, which must satisfy V_{aN}+ V_{bN}+V_{cN}= 0 and V_{bN}=V_{cN}.

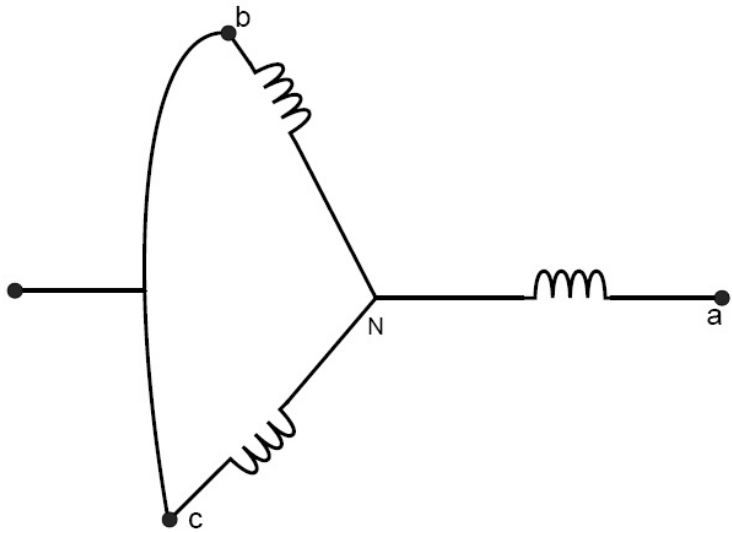

Figure 4.13: *Reference frame diagram*

Therefore the assumption seen in equations 4.14 and 4.15 can be stated.

$$V_{aN} = -2V_{bN} = -2V_{cN} \tag{4.14}$$

$$V_{ab} = V_{aN} - (-\frac{V_{aN}}{2}) = \frac{3}{2}V_{aN} \tag{4.15}$$

Using the above equation new expressions for d and q voltages are found as in equation 4.16 and 4.17.

$$V_d = -\frac{2}{3}[cos(\theta)V_{aN} - cos(\theta - \frac{2\pi}{3})V_{bN} - cos(\theta + \frac{2\pi}{3})V_{cN}) = V_{aN} \cdot cos(\theta) \tag{4.16}$$

$$V_q = -V_{aN} \cdot sin(\theta) \tag{4.17}$$

From the voltage equations 4.18 of machine at zero speed the expression for d and q current are found as in equations 4.19 and 4.20.

$$V_d = R_{id} + L_d\frac{d_{id}}{dt}; V_q = R_{iq} + L_q\frac{d_{iq}}{dt} \tag{4.18}$$

$$i_d = \frac{V_d}{R}(1 - e^{-\frac{t}{\sigma_d}}) \tag{4.19}$$

$$i_q = \frac{V_q}{R}(1 - e^{-\frac{t}{\sigma_q}}) \tag{4.20}$$

where $\sigma_q = \frac{L_q}{R}$ and $\sigma_d = \frac{L_d}{R}$

Using the expression for the current on phase a (i_a) like in equation 4.21 and because i_a+i_b+i_c=i_0 results that i_0=0 .

$$i_a = cos(\theta)i_d - sin(\theta)i_q + i_0 \tag{4.21}$$

Substituting the d and q currents in equation 4.22 the new expression for i_a is found.

$$i_a = \frac{cos^2(\theta) \cdot V_{an}}{R} \cdot (1 - e^{-\frac{t}{\sigma_d}}) + \frac{sin^2(\theta) \cdot V_{an}}{R} \cdot (1 - e^{-\frac{t}{\sigma_q}}) \tag{4.22}$$

In Fig 4.15 the components used for inductance measurement are presented. The computer is used to control the step motor with the desired angle, while the DC source is used to apply the IPMSM with voltage.

The torque transducer and the fluke are used to measure the torque and voltage, while the current can be read from the DC source. The high values resistor and the variable resistors are used to limit the current when the Ampere switch is turned on.

The purpose of this measurement is to register the transient period for a step current and voltage. This is done using the oscilloscope. For example if the current is set to 10 [A], the oscilloscope should register the data only for the step current from 10[A] to 9[A].

If the transient period is obtained the inductance L_d and L_q can be found using the mathematical approach described above and implemented in the program from Apendix B.3.

In Fig 4.14 the data for a step current is stored using the oscilloscope. The transient period begin form 4.4[A] and is terminated until 3.4[A]. If the values for inductance are obtained then currents I_d and I_q in function of flux or the other way around can be seen.

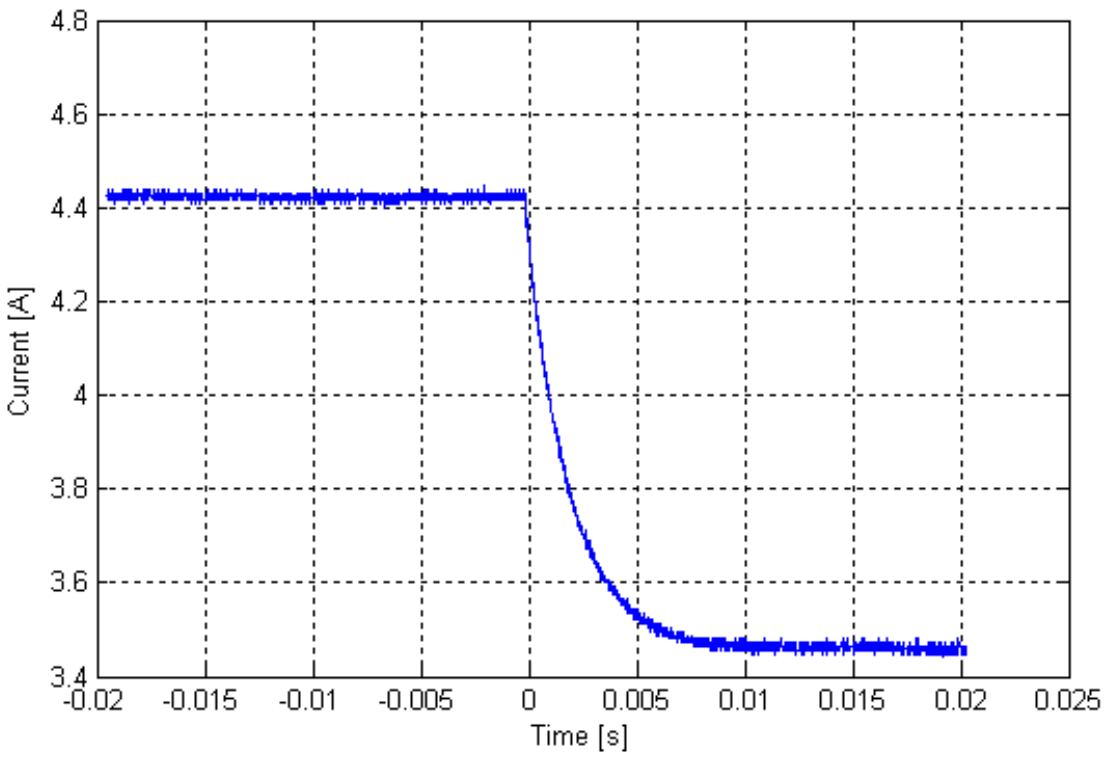

Figure 4.14: *Current transient period from 4.4[A] to 3.4[A]*

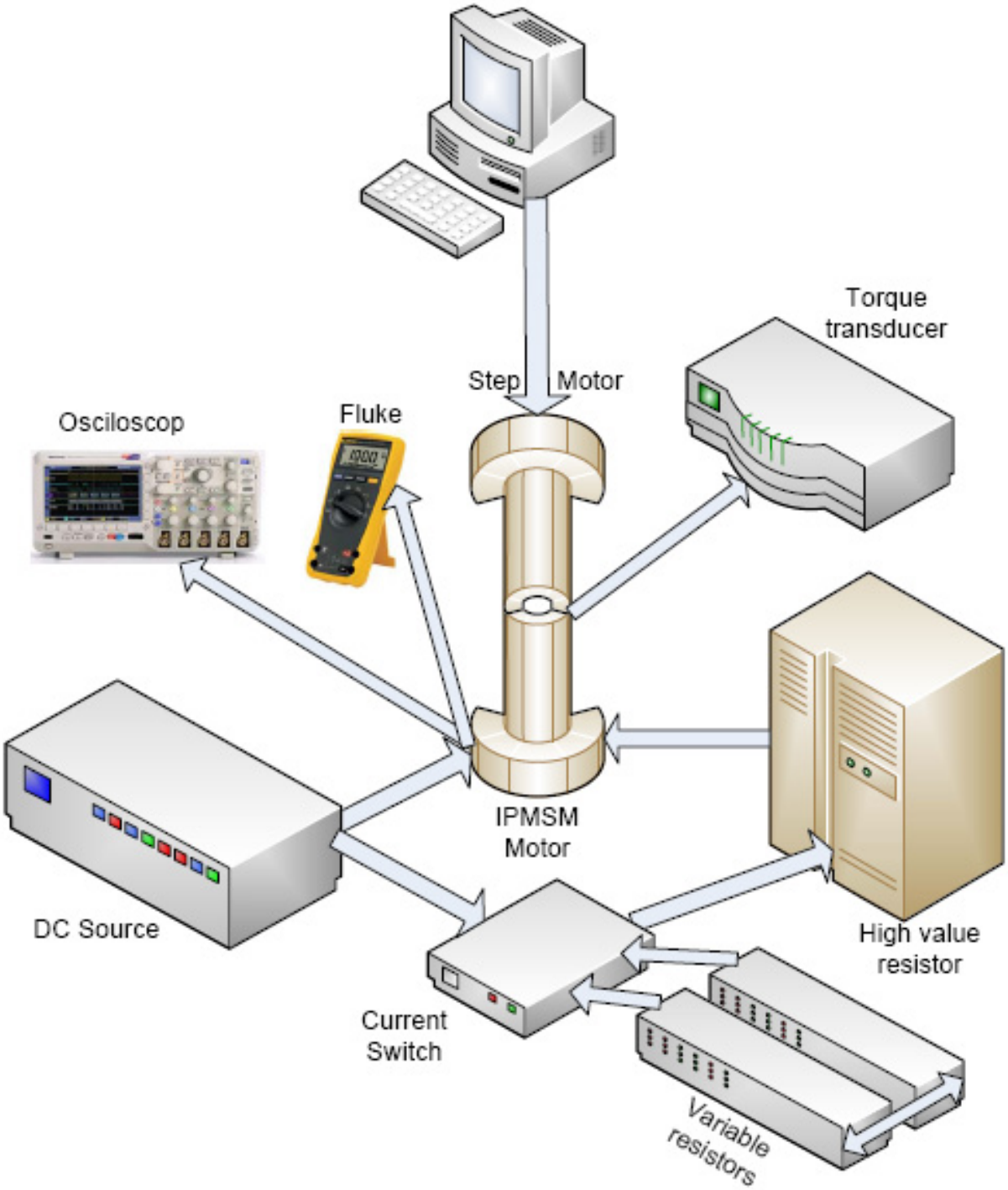

Figure 4.15: *Scheme of components used for inductance measurement*

In Fig 4.16 the laboratory setup used in the experiment can be seen.

Figure 4.16: *Test setup used for inductance measurement*

Because of time constraints the inductance measurement data couldn't be processed. The data from [15] was used instead. The figures obtained are for different data than the ones obtained in laboratory but the waveform shapes and principle should be the same.

In Fig 4.17 and 4.18 the flux ψ_d and ψ_q are in function of I_d and I_q. Figure 4.17 show a high coupling between ψ_d and I_q especially for negative high values of I_d . Figure 4.18 show a low coupling between ψ_q and I_d. Therefore the cross saturation phenomenon is fundamental for modeling IPMSM.

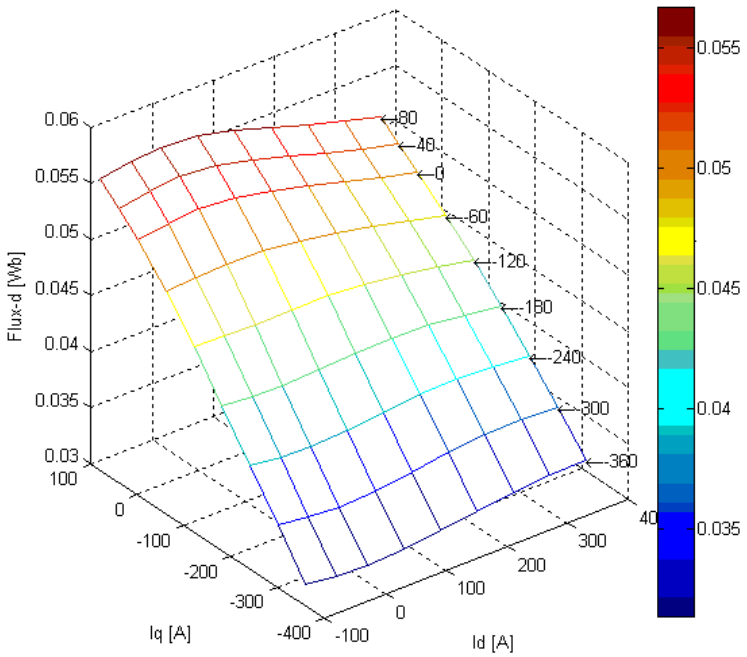

Figure 4.17: *Flux ψ_d function of currents I_d, I_q*

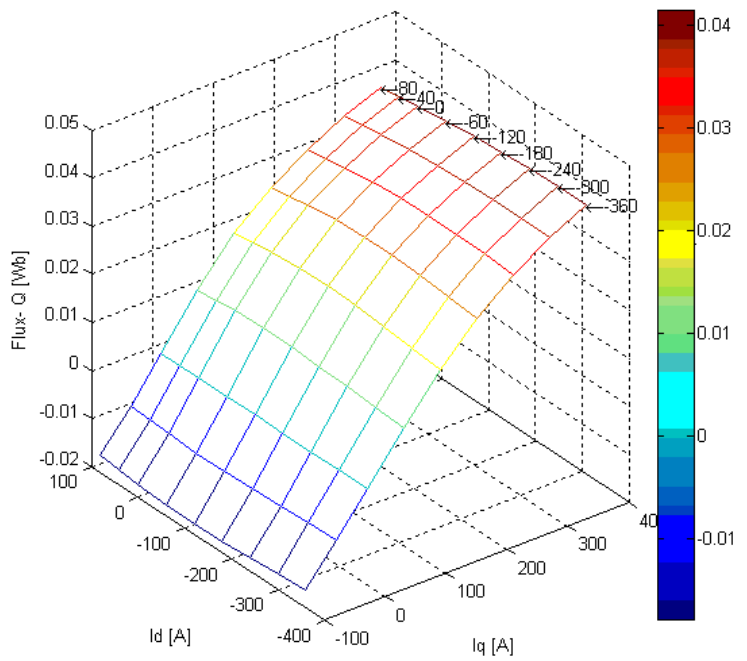

Figure 4.18: *Flux ψ_q function of currents I_d, I_q*

Chapter 5

Conclusion

The main objective of this project was the investigation of saturation effect of an IPMSM motor by measuring the torque and inductances. The report is divided in five main chapters.

All the objectives and limitations of the project are stated in the first chapter. The second chapter presents the mathematical model and of IPMSM and also the simulation which is done in order to validate the model.

In the third chapter different control strategies and control property are described. Field Oriented Control was chosen to be implemented in simulation and MTPA as control property. MTPA were simulated for different inductances values in order to observe the saturation effect.

The PI controllers were designed and simulations were carried out for different step in speed and torque. Steady state model was also made in order to see the behavior of inductance as a function of current. Saturation effect was included by using two look up tables.
It can be stated that when the saturation point is reached the inductances are decreasing when current reach bigger values.

In laboratory chapter torque measurement and inductance measurement were carried out. First the description of the procedure was explained , followed by the setup used.

From the torque measurement was observed that a cross-coupling phenomenon appears in the measured torque which in calculated torque cannot be seen. Also the flux $_d$ and flux $_q$ in function of I_d and I_q plots were done using the data from [15].
It can be stated that a low coupling between I_d and flux $_q$ appear while high coupling between I_q and flux $_d$ can be noticed.

In conclusion it can be stated that a cross coupling between d and q axis appears. Thus the two axis frame model of a saturated machine cannot be handled separately.

Future work

Because not all the goals of this project were reached, there are several topics which can be analyzed as future work. The topics which can be investigated are:

- A dynamic simulation with saturation effect included and implemented in laboratory.
- Design of the inductance saturation compensation function.
- Validation of dynamic Simulink model in dynamic tests using a control platform.
- A sensorless control of IPMSM can also be investigated.

Bibliography

[1] "Sensorless Control of Permanent Magnet Synchronous Motor Drives", Chandana Perera, PHD Thesis, December 2008, Aalborg University.

[2] "Electrical Machines And Drives", Peter Vas, ISBN: 0198593783, 1993-02-25.

[3] "Modeling and analysis of permanent magnet synchronous motor by taking saturation and core loss into account", Wijenayake, A.H. Schmidt, P.B, Power Electronics and Drive Systems, 1997 Proceedings, 1997 International Conference, 26-29 May 1997.

[4] "Stability Limits of Saturated Interior Permanent Magnet Motors", Essam Eddin M. Rashad, IEEE PEDS 2005, December 2008.

[5] "Evaluation of Saturation and Cross-Magnetization Effects in Interior Permanent Magnet Synchronous Motor", Bojan Stumberger, Gorazd Stumberger, Drago Dolinar, Anton Hamler, Mladen Trlep, 2000 Maribor, Slovenia.

[6] "Experimental Method for Determining Magnetically Nonlinear Characteristics of Electric Machines With Magnetically Nonlinear and Anisotropic Iron Core, Damping Windings, and Permanent Magnets", Gorazd Stumberger, Tine Marcic, Bojan Stumberger, Drago Dolinar, TECES, Research and Development Centre of Electrical Machines, Pobreska cesta 20, 2000 Maribor, Slovenia.

[7] "Modern power electronics and AC drives", Bimal K. Bose, Prentice Hall PTR 2001, ISBN 0-13-016743-6.

[8] "Fundamentals of polyphase electric motors", Lincoln electric, Journal,june 2005.

[9] "Modification of Symmetric Optimum Method", R.Mizera, ASR 2005 Seminar, Instruments and Control, Ostrava, April 29, 2005.

[10] "Feedback Control of Dynamic Systems-Fifth Edition", G. F. Franklin, J. D. Powell, A. Emami-Naeini, Pearson Prentice Hall 2006, ISBN: 0-13-149930-0.

[11] "ADSP-21990:Reference Frame Conversion",Analog Devices,Journal-January 2002.

[12] "Compact Field Weakening Controller Implementation", J.Ottosson, M.Alakula, SPEEDAM 2006 International Symposium on Power Electronics, Electrical Drives, Automation and Motion

[13] " Electric Drives", I.Boldea, S.A.Nasar, CRC Press 1999.

[14] " Control in Power Electronics Selected problems", IM.P. Kawmierkowski, R. Krishnan, Academic Press, USA, 2002, ISBN 0-12-402772-5.

[15] " Modelling Magnetic Saturation Effects in IPMSMs for use in Sensorless Saliency Based Methods", Torben N. Matzen, Peter O. Rasmussen, Aalborg University, Denmark.

[16] " Experimental study of the saturation and the cross magnetizing phenomenon in saturated synchronous machines ", A.M El-Serafi, IEE Transaction on Energy Conversion, Vol 3, No4,December 1998.

[17] " Saturation Modelling in D-Q axis models of salient pole Synchronous Machines ", E. Levi, IEE Transaction on Energy Conversion, Vol 14, No1,March 1999, Liverpool University.

[18] " A cross saturation model for interior permanent magnet synchronous machine. Application to a starter-generator ",L. Chedot, G. Friedrich, IEE Transaction on Energy Conversion,2004.

Nomenclature

u_{sd}, u_{ds}	D-axis stator voltages	$[V]$
u_{sq}, u_{qs}	Q-axis stator voltages	$[V]$
u_{sqd}, u_{sdq}	DQ-axis stator voltages	$[V]$
i_{sd}, i_{ds}	D-axis stator currents	$[A]$
i_{sq}, i_{qs}	D-axis stator currents	$[A]$
i_{sdq}, i_{sqd}	dq-axis stator currents	$[A]$
i_{α}, i_{β}	$\alpha\beta$ currents	$[A]$
L_d, L_q	D and q-axis stator inductances	$[H]$
L_{md}, L_{mq}	D and q magnetizing inductances	$[H]$
L_{aas}, L_{bbs}, L_{ccs}	Stator self inductances	$[H]$
L_{abs}, L_{acs}	Stator mutual inductances	$[H]$
L_{md}, L_{mq}	D and q magnetizing inductances	$[H]$
R_s	Stator resistance	$[\Omega]$
ω_m	Mechanical speed of the rotor	$[rad/s]$
ω_e	Electrical speed of the rotor	$[rad/s]$
ψ_m	Permanent magnet flux linkage	$[Wb]$
ψ_s	Stator flux linkage	$[Wb]$
ψ_d	D axis flux linkage	$[Wb]$
ψ_q	Q axis flux linkage	$[Wb]$
ψ_{abcs}	Stator flux linkage matrix	$[Wb]$
i_{abcs}	Stator phase currents matrix	$[A]$
v_{abc}	Stator phase voltage matrix	$[A]$
T_e	Electromagnetical torque	$[Nm]$
p	Number poles	$-$
n_{pp}	Number of the pole pairs	$-$
n_s	Synchronus speed	$[rad/s]$
f	Frequency	$[Hz]$
T_L	Load torque	$[Nm]$
J	Moment of inertia	$[kg \cdot m^2]$
B_m	Viscous friction	$[Nms]$
i_{abc}	Line currents	$[A]$
V_{DC}	DC - voltage	$[V]$
I_{DC}	DC - current	$[A]$
P_e	Electrical power	$[W]$
P_{em}	Electromechanical power	$[W]$
P_m	Mechanical power	$[W]$
θ	Rotor position	$[rad]$

ζ	Damping ratio	$-$
k_p	Proportional gain	$-$
k_i	Integrator gain	$-$
T_i	Integrator time	$[s]$
$G_c(s)$	Pi transfer function	$-$
$G_p(s)$	Transfer function of the plant	$-$
$G_{ol}(s)$	Open loop transfer function of the plant	$-$
$G_{om}(s)$	Second oreder transfer function	$-$
T_s	Time constant	$[s]$
t_s	Settling time	$[s]$
f_s	Sampling frequency	$[Hz]$
f_{inv}	Inverter frequency	$[Hz]$
T_{inv}	Inverter delay time constant	$[s]$
T_{si}	Equivalent time constant	$[s]$
k_{pi}	Proportional gain for currents controller	$-$
τ_q, τ_d	Rise time	$[s]$
$T_{wc}(s)$	Filter time constant for speed controler	$[s]$
T_{sw}	Equivalent time constant for speed controler	$[s]$
T_w	Integrator time for speed PI controller	$-$
k_{pw}	Proportional gain for speed controller	$-$

Acronyms

AC	Alternating Current
DC	Direct Current
CTA	Constant Torque Angle
DTC	Direct Torque Control
FOC	Field Oriented Control
V/Hz	Volt/Hertz
VSI	Voltage Source Inverter
$PMSM$	Permanent magnet Synchronous Machine
$IPMSM$	Interior Permanent magnet Synchronous Machine
$SPMSM$	Surface Permanent magnet Synchronous Machine
$PMDC$	Permanent Magnet Direct Current
$PMAC$	Permanent Magnet Alternating Current
$BLDCM$	Brushless Direct Current Motor
PI	Proportional Integral
EMF	Electromagnetic force
PF	Power Factor
SVM	SPACE Vector Modulation
PWM	Wind speed
GM	Gain Margin
PM	Phase Margin

Appendix A

Simulink Model

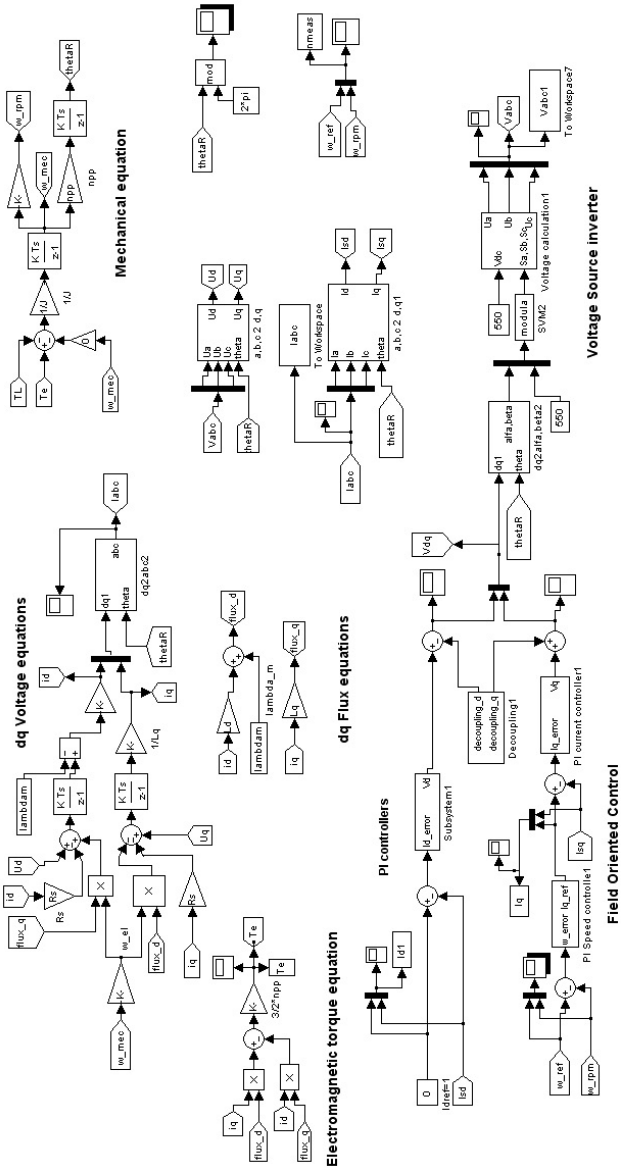

Appendix B

M-File

B.1 Torque Calibration M-file

```
clear all;
clc;

Weight = [-3.9, -3.7, -3.4, -3.2, -2.9, -2.7, -2.4, -2.2, -1.9,-1.7,
          -1.4, -1.2, -0.9, -0.7, -0.4, -0.2, 0, 0.2, 0.4, 0.7, 0.9,
          1.2, 1.4, 1.7, 1.9, 2.2, 2.4, 2.7, 2.9, 3.2, 3.4, 3.7, 3.9];
ArmLength        = 52e-2;
Kg               = 9.8;

T_actual = Weight*Kg*ArmLength

T_mes = [-20.15 -19.11 -17.58 -16.52 -14.98 -13.9 -12.38 -11.35 -9.8
         -8.76 -7.21 -6.17 -4.63 -3.59 -2.05 -1 0 1.1 2.15 3.7 4.75 6.29
         7.33 8.9 9.92 11.46 12.5 14.04 15.09 16.62 17.66 19.21 20.26];
% - torque
figure;          hold on;        grid on

plot(Weight, T_actual, 'ro-')
plot(Weight, T_mes , 'bs-')
```

B.2 Torque Measurement M-file

```
clear
Id                  = [-19 -15 -12 -8  -4  0 3 6 10];
Iq                  = [2 4 7 10 15 20  23 27 30];

for i = 1:length(Id)
    for j = 1:length(Iq)
        the(i,j) = -atan2(Iq(j),Id(i));
        if abs(abs(the(i,j)) -pi/2) > 1e-8
        Ia(i,j)  = Id(i)/cos(the(i,j));
              else
        Ia(i,j)=Iq(j);
              end
    end
end
Id_cal              = +2/3.*(cos(the).*Ia+cos(the-2*pi/3).*
                      (-Ia/2)+cos(the+2*pi/3).*(-Ia/2));
Iq_cal              = -2/3*(sin(the).*Ia+sin(the-2*pi/3).*
                      (-Ia/2)+sin(the+2*pi/3).*(-Ia/2));

omega               = 2*pi*1000*3/60;
Lndmpm              = 41/sqrt(3)/omega;

Trq                 = 3/2*3*(Lndmpm*Iq_cal+(3.2-4.1)
                      *1e-3*Iq_cal.*Id_cal);
the                 = the*180/pi;
step= the/(0.18*3);
```

B.3 Ld,Lq Measurement M-file

```
% To use the transient current waveform in response to
%a step voltage change for Ld, Lq estimation.
clear

global              Vab theta Rs

Rs                  = 8.5*1;

Ld                  = 51e-3;                          % [H]
Lq                  = 81e-3;                          % [H]

% theta = pi/4
% save Transient_Vi_19052010_1 Vab_ws ia_ws theta
load Transient_Vi_19052010_1
t                   = Vab_ws.time;
Vab                 = Vab_ws.signals.values;
ia                  = ia_ws.signals.values;
LdLqini             = [Ld, Lq]*0.8;
[estimates, model]  = LdLq_est_subfunc(t,ia, LdLqini);
[sse, FittedCurve]  = model(estimates);

tord_est            = estimates(1);
torq_est            = estimates(2);
Ld_est              = tord_est*Rs;
Lq_est              = torq_est*Rs;

E                   = 2/3*Vab(length(Vab));
ia_est              = cos(theta)^2/Rs*E*(1-exp(-t/tord_est))
                     +sin(theta)^2/Rs*E*(1-exp(-t/torq_est));
hold on;            grid on
plot(t,ia,'r');
plot(t,ia_est,'g')
disp([Ld Ld_est Lq Lq_est])
```

B.4 MTPA M-file

```
% MTPA file, for variable Ld,Lq inductances.
clear all;
clc;
flux_m = 0.08;
npp = 3;
Ld = 3.2e-3;
Lq = 4.1e-3;
Isn = 30;
k=1;
for is=0:0.1:Isn
a=[2 flux_m/(Ld-Lq) -is*is];
R=roots(a);
if(R(1)<R(2)), id=R(1);
else
id=R(2);
end
iq=sqrt(is*is-id*id);
te=1.5*npp*(flux_m+(Ld-Lq)*id)*iq;
Id(k)=id;
Iq(k)=iq;
Te(k)=te;
i=is;
k=k+1;
end
x=[Te;Id];
y=[Te;Iq];
plot(Te,Iq)
```

Appendix C

Contents of CD-ROM

- Articles:
  This folder contains all the articles used as references in the bibliography.
- Laboratory results:
  This folder contains all the data measured in the laboratory.
- Report files:
  This folder contains a pdf version of the project and all the Latex files.
- Simulation files:
  This folder contains all Matlab and Simulink files used in the report.